An Energy-Aware Optimization Model for the Water-Based Lithium-Ion Battery Electrode Drying Process

By

Mohammad Aldabbas

Submitted in Partial Fulfillment of the Requirements

For the Degree of

Master of Science in Engineering

In

Industrial and Systems Engineering

YOUNGSTOWN STATE UNIVERSITY

May 2024

An Energy-Aware Optimization Model for the Water-Based Lithium-Ion Battery Electrode Drying Process

Mohammad Aldabbas

I hereby release this thesis to the public. I understand that this thesis will be made available from the OhioLINK ETD Center and the Maag Library Circulation Desk for public access. I also authorize the University or other individuals to make copies of this thesis as needed for scholarly research.

Signature:

_____

Mohammad Aldabbas, Student Date

Approvals:

_____

Seokgi Lee , PhD, Thesis Advisor Date

_____

Cory Brozina, PhD, Committee Member Date

_____

Kyosung Choo, PhD, Committee Member Date

_____

Salvatore A. Sanders, PhD, Dean, College of Graduate Studies Date

Abstract

Lithium-ion batteries (LIBs) have been a vital technology since they were introduced to the world in the 1990s. Despite significant advancements in cost-effectiveness and production efficiency, there are still some obstacles that need to be addressed. Significantly, as lithium-ion battery (LIB) technology is increasingly used in the transportation industry to enable electric vehicles, the issue of industrial ethics and environmental sustainability becomes of extreme importance. We are currently developing water-based manufacturing procedures to achieve more environmentally friendly production of lithium-ion batteries. Our research focuses on analyzing the design elements and process dynamics involved in removing solvents from the electrode coatings of these batteries. We demonstrate the impact of substituting N-Methyl-2-pyrrolidone (NMP) with an aqueous solvent, specifically water, in the electrode. To describe the process of cathode drying, we employ a mathematical model at the continuous level. This model accounts for the simultaneous transmission of heat and mass, as well as phase change. The utilization of aqueous processing for electrode material has the potential of cost reduction and environmental effect reduction in existing lithium-ion battery (LIB) manufacturing processes. By substituting costly and hazardous binder solvents like N-methyl-2-pyrrolidone (NMP) with water-based processing, both material expenses and processing and capital equipment costs can be minimized. The optimization model will determine the most efficient factors for the energy consumption of the solvent drying process, which constitutes a significant component of the overall energy consumption in the drying process.

Table of Contents

LIST OF FIGURES

List of Tables

Chapter 1

Introduction

Transportation is widely recognized as a significant environmental challenge with detrimental implications for humanity. This is mostly attributed to the fact that transportation stands as one of the largest contributors to emissions, ultimately increasing the issue of global warming. Furthermore, the growing demand for electric vehicles and batteries can be attributed to both legislative requirements and market adaptability towards more ecologically sustainable products (McManus, M. C. 2012, January 13). The issue of greenhouse gas emissions resulting from transportation has posed a significant and enduring challenge for governments. Finding an environmentally friendly alternative to internal combustion engines has been a primary objective for many developed nations, prompting substantial financial investments to incentivize automobile manufacturers to produce feasible and competitive alternatives. In 2010, Tesla was granted a loan of $465 million by the Loan Programs Office of the United States Department of Energy (US DOE), as evidenced by official records. Additionally, the United States government has formulated a strategy to reduce emissions by 50%–52% by the year 2030, with the ultimate objective of achieving complete emission neutrality by 2050. The Infrastructure Investment and Jobs Act, enacted in November 2021, included a provision that designates $7.5 billion for the development of a comprehensive charging infrastructure across the United States (The United States Government, 2021, November 8). This allocation aims to stimulate the adoption and use of electric vehicles (EVs) by enhancing the accessibility and convenience of charging facilities. The rise in gasoline prices, government regulations, extensive charging infrastructure, and advancements in battery technology have contributed to a significant surge in the adoption of electric vehicles (EVs). This growth has intensified competition among EV manufacturers,

particularly in the industry of battery production. Batteries are considered an essential component of EV technology, as they play a pivotal role in attracting customers through their capacity, range, and longevity. The electric vehicle (EV) battery constitutes around 30% of the overall cost of EVs, making it a significant determinant of the EV price. According to a report by Bloomberg New Energy Finance, the cost of EV batteries has experienced a 7% increase in 2022 compared to the preceding year (Henze, V., 2022, December 6). Electric vehicles (EVs) that utilize lithium-ion batteries are primarily designed to reduce greenhouse gas emissions associated with ground transportation. However, it is important to note that EVs do contribute to greenhouse gas emissions indirectly through the energy consumption of the battery pack, which includes the embedded energy from the manufacturing process of lithium-ion batteries. The increasing need for full evaluations of the environmental consequences associated with this technology requires the determination of the energy and materials utilized during its production. Furthermore, there have been major advancements in battery cell manufacturing, particularly during the past two decades. Nevertheless, given the variety of sequential process steps, the interplay between these stages, and the significant number of individual process parameters involved, it is reasonable to believe that there exists an opportunity for additional optimization (Duffner, F., Mauler, L., Wentker, M., Leker, J., & Winter, M. 2021).

1.2 Manufacturing Process

Manufacturing Process Lithium-ion batteries, which rely on lithium cobalt oxide ($LiCoO_2$), are employed in electric vehicles. The extraction of lithium ions from the molecule and their subsequent pairing with graphite is a process that occurs with relative ease. The movement of lithium ions across the separator toward the positive anode and the negative cathode makes it easier for free electrons to form, which then provide the device with the power

it needs to work. The initial step in the production of these batteries is the blending of raw ingredients to form the electrode. The aforementioned raw materials encompass metallic elements like iron, nickel, and cobalt, alongside non-metallic elements like graphite, lithium, and manganese. After being thoroughly mixed, the electrode material is subsequently applied as a coating to sheets of copper and aluminum foil. Subsequently, the separator and electrode components are interconnected to form the electrochemical cell. Typically, the production of lithium-ion battery cells is differentiated by a substantial number of operations, which can be grouped into three basic stages: the manufacture of electrodes, the assembling of cells, and the finishing of cells. The manufacturing process for lithium-ion batteries is further divided into three main production zones, as seen in Figure 1. Each of these stages contains various sub-processes, beginning with the application of a coating to both the anode and cathode, followed by the assembly of different elements, and ending in the packaging and testing of the lithium-ion battery cells. The three primary types of cells that are often manufactured include prismatic, cylindrical, and pouch cells. While there are variations in the design of these cells, the manufacturing procedures employed for their production are generally comparable. The manufacturing expenses associated with battery cells are a crucial determinant, as they constitute approximately 20% to 25% of the overall lithium-ion battery expenditure (Conlon, D. 2022, February 10).

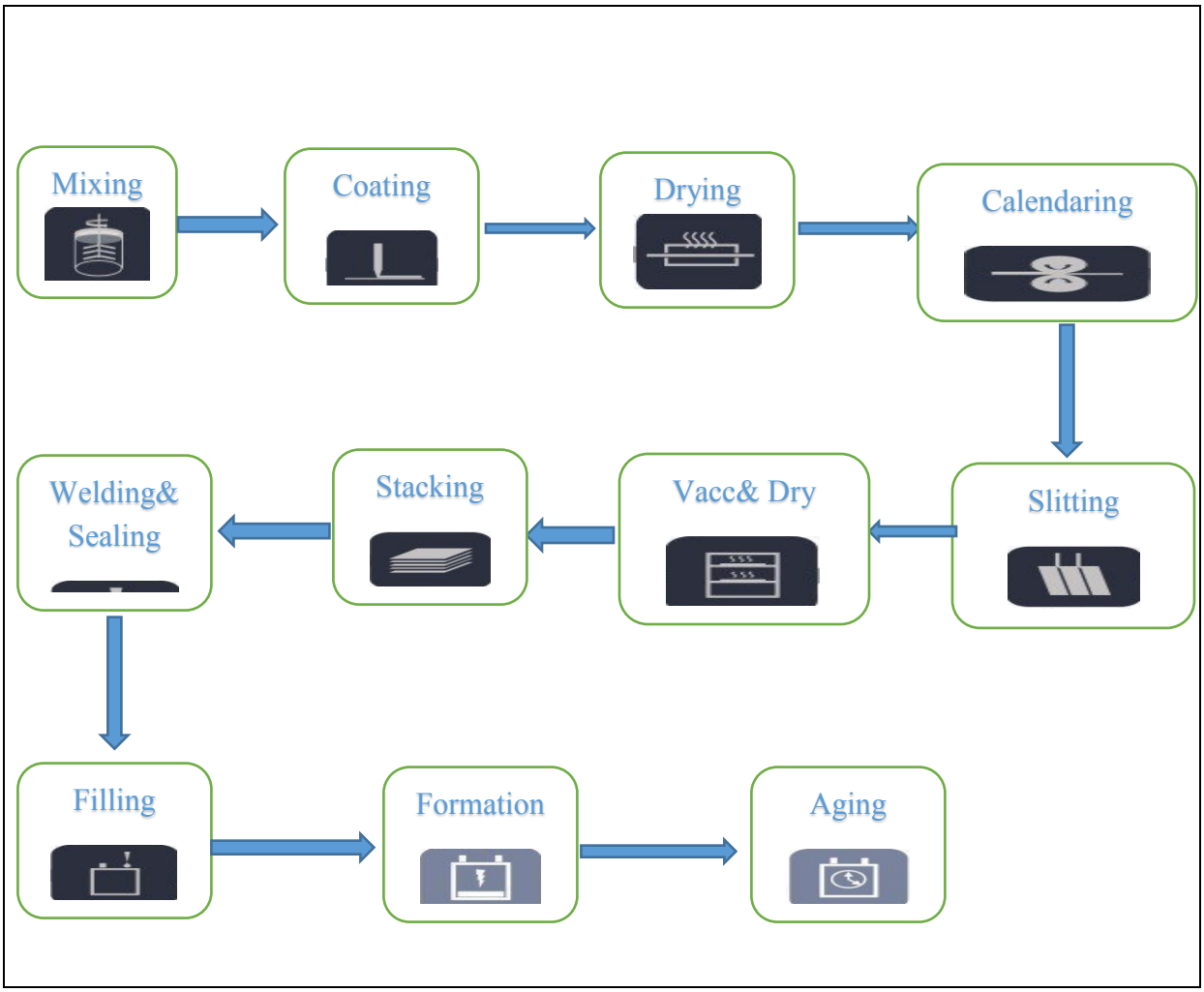

Figure 1 lithium ion battery cell production process

1.3 Electrode Manufacturing

By using a conductive binder, the aim is to produce a uniform slurry by mixing it with the solvent. Following that, Thomitzek, M., Cerdas, F., Thiede, and Herrmann (2019) describe applying the slurry to both sides of the current collector using aluminum foil for the cathode and copper foil for the anode. The application of this coating can be performed in a continuous or intermittent manner. The coating equipment is supplied with the capacity to modify the thickness of the coating that is applied to the electrode. After the solvent has evaporated, the foil that has

been coated is immediately moved into a larger drying oven. After this, the calendaring process begins, in which a sequence of revolving rollers exert pressure on the coated foils to achieve compression. This process enables the modification of many physical characteristics of the electrodes, including adhesion, conductivity, density, and porosity, among other factors (Gupta, N. 2021, June 11). Afterward, the electrodes that have been manufactured are subjected to a cleaning process before to being inserted into slitting machines. The electrodes in these devices are precisely cut into small strips and then tightly twisted into coils. This operation takes place after the calendaring process. After processing, a vacuum oven is used to remove any leftover solvent and moisture from the coils.

1.4 Cell Assembly

Once the necessary preparations are finished, the electrodes are transferred to a specially designed dry chamber where the sub-assembly technique is conducted. In this stage, a separator material is precisely placed between the anode and the cathode, leading to the creation of the internal structure of the cell. Depending on the specific type of cell being used, either a stacking electrode structure for pouch cells or a winding electrode structure for prismatic and cylindrical cells can be employed (Gupta, N. 2021, June 11). The selection between these two fundamental electrode topologies is based on the particular cell configuration under consideration. The constructed cellular structure is subsequently linked to the terminals or cell tabs by ultrasonic or laser welding methods. All essential safety precautions are integrated into these components. This operation takes place once the electrode assembly has been finished. Subsequently, the process involves injecting the electrolyte into the enclosed cell, which is then sealed securely. It is crucial to emphasize that the entire procedure is conducted in a dry environment to avoid the breakdown of the electrolyte, which might potentially lead to the release of hazardous gases.

1.5 Cell Finishing

The formation process refers to the initial charging and discharging cycles of a battery cell following the injection of electrolyte into it. The cells are positioned in data racks and connected through contact pins that are spring-loaded. Subsequently, the cells undergo charging or discharging processes in accordance with carefully calculated current and voltage curves. In the course of this particular procedure, lithium ions are incorporated within the crystalline structure of the graphite material situated on the anode side. This integration gives rise to the development of a safeguarding layer known as the Solid Electrolyte Interface (SEI), which acts as a barrier between the electrolyte and the electrode (Guo, Y. 2009). The presence of a protective coating contributes to the reduced self-discharge of lithium-ion batteries and exerts an influence on both battery performance and lifetime. Following the process of formation, the subsequent stage is known as aging, which is carried out with the intention of enhancing the overall quality. The process of aging involves the continuous monitoring of cell properties and cell performance by means of regular measurement of the open-circuit voltage (OCV) of the cell for a duration of up to three weeks. A differentiation is established between high-temperature (HT) and normal-temperature (NT) aging. Typically, cellular aging proceeds through a sequence of high-temperature (HT) aging followed by normal-temperature (NT) aging. The process of formation and aging represents 32 percent of the overall production procedure (Gupta, N. 2021, June 11).

1.6 Energy Consumption Breakdown

Information regarding the specific details of battery manufacturing processes is readily accessible within the industry but slightly scarce within the scientific community or public domain. In addition, it should be noted that various stages involved in the battery production process exhibit distinct energy and material requirements, thereby leading to varying levels of global warming potential (GWP) emissions (Jinasena, A., Burheim, O. S., & Strømman, A. H. 2021). The primary cause of the significant variability observed in the data derives from the utilization of generalized data across battery production processes that naturally differ from one another. The majority of the data available relies on estimations or outdated plant data, rendering it unsuitable for application to modern plants that possess significantly greater capacity and employ various technologies and materials. The energy requirements of production systems are subject to variation based on several factors, including the factory's capacity, geographical location, battery cell type, energy, and chemistry, as well as the specific technologies applied. A series of studies were done to assess the energy consumption associated with the manufacturing process of various plants and cells. These studies can be summarized and represented in Figure 2 (Nigel, 2022, October 11). Several researchers conducted studies to determine the energy consumption associated with the manufacturing process of lithium-ion batteries, as an illustrative example. Jinasena provides a comprehensive analysis of the existing studies conducted thus far. Based on this analysis, the authors develop a model and show significant empirical findings (Jinasena, A., Burheim, O. S., & Strømman, A. H. 2021). Simon Davidsson has provided a comprehensive synthesis of much research, examining the Northvolt and Tesla Gigafactories, yielding an estimated range of 50 to 65 kWh (el)/kWh (c). The initial point of reference pertains

to the examination of energy consumption in large-scale cell manufacturing facilities, which is of particular significance due to the predominant presence of such plants in the cell manufacturing sector. The researchers reach the conclusion that the energy expenditure associated with the production of diverse chemical compositions amounts to 47.23 ± 13.03 kWh (el)/kWh (c). The cathode process uses 37% of the total energy required, with the drying process consuming the majority of the energy. The anode process uses 12% of the total energy, the majority of which is used in the drying process. During these stages, a significant amount of energy is used for cell assembly and finishing, 51% of the total energy is used, 47.8% is used in the dry room, and 3.3% is used in cell formation (Nigel, 2022, October 11).

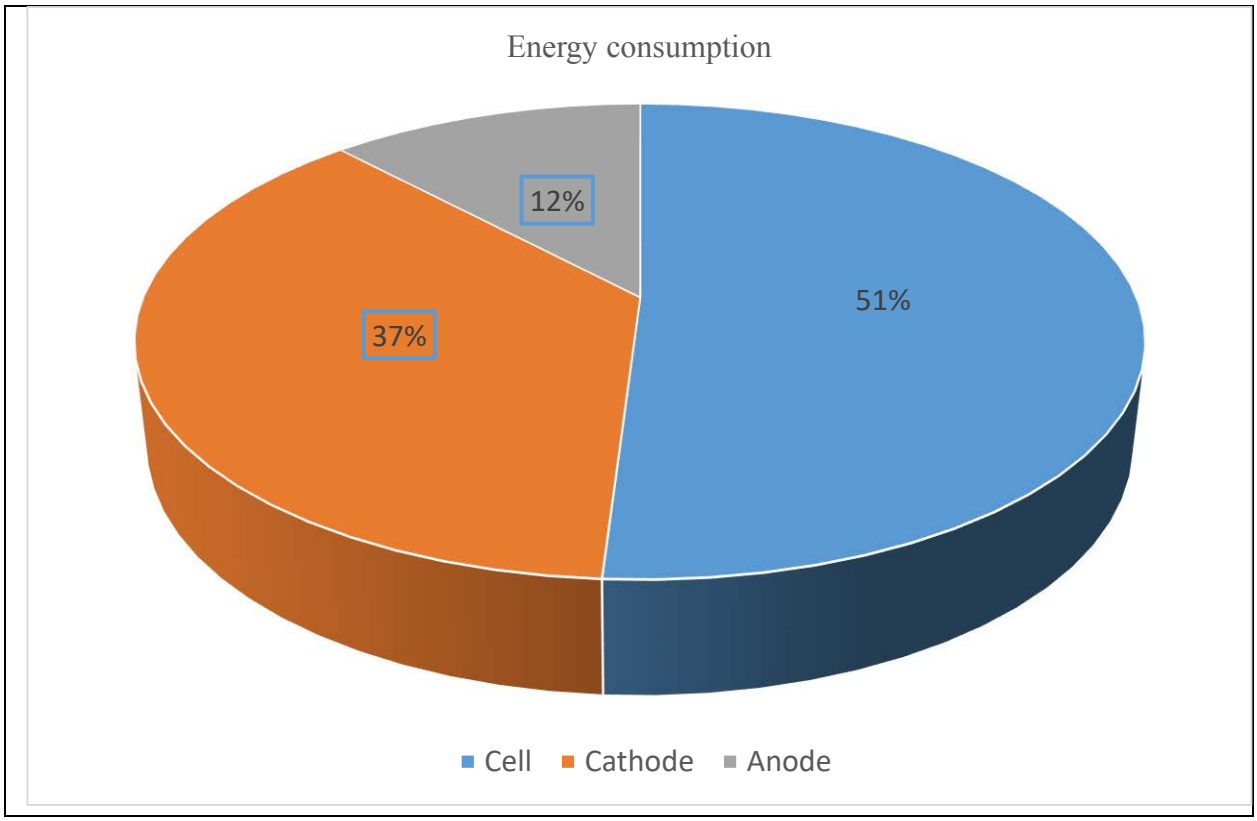

Figure 2 Energy Consumption Breakdown illustrated by the author.

Nigel didn't take into consideration the minor energy expenditure associated with certain sub-processes, such as mixing, coating, stacking, welding, sealing, and others. By incorporating these marginal percentages, a comprehensive assessment of energy consumption can be derived, as illustrated in Figure 3 and Figure 4.

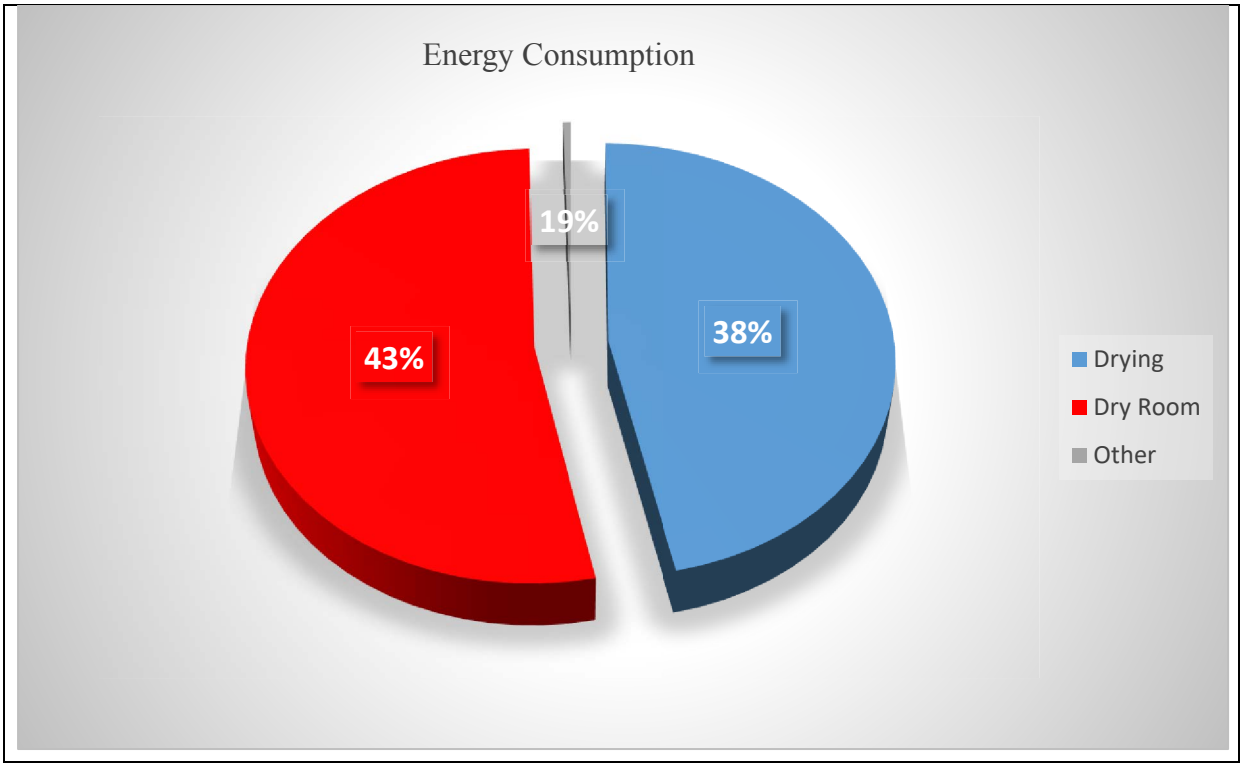

Figure 3 Energy Consumption Breakdown illustrated by the author.

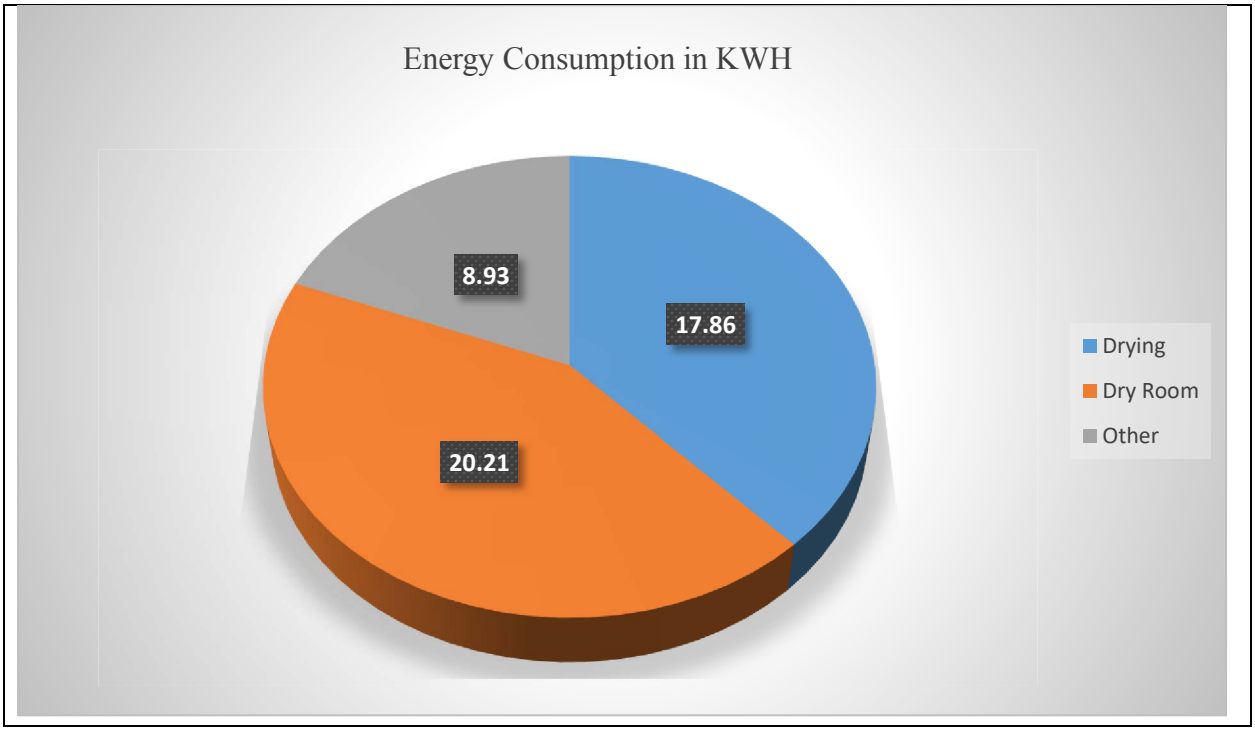

Figure 4 Energy Consumption Breakdown in KWH illustrated by the author.

According to the findings, the production of lithium-ion batteries requires an estimated energy consumption of approximately 47.23 kWh (el)/kWh (c); in other words, we need about 47 kWh of energy to manufacture 1 kWh of battery. This number was derived from the study's findings. It is essential to point out that this number does not take into account the amount of energy that was wasted in the mining, refining, or processing of the raw materials in advance of their use in the cell manufacturing plant. The annual expected amount of power that would be used by the 35 GWh production line is predicted to be between 1653 and 455 GWh. The dry room and the process of drying the cathode and anode each consume a significant percentage of the total amount of energy that is being generated.

1.7 Research Objective

As a direct result of the ever-increasing demand for battery-powered electric vehicles across the globe, there has been a discernible increase in the annual building of lithium-ion battery production facilities (also known as LIB). The development of lithium-ion batteries, often known as LIBs, has a number of significant obstacles, the most significant of which are the high electrical energy consumption and large investment costs involved with the drying process employed in the creation of solvent-based electrodes. During the coating process, there is a rising interest in the development of innovative electrode drying technologies that can speed up the drying process and increase the coating process's ability to transfer heat efficiently. This interest is the result of a desire to meet the requirements for the conservation of energy, the reduction of CO_2 emissions, and the lowering of costs associated with the production of lithium-ion batteries. Zackrisson et al. conducted a study and found that there is a noteworthy environmental advantage associated with the production of a 10 kWh battery pack. Specifically, they established that the life-cycle CO_2 emissions can be greatly reduced through the use of aqueous processing compared to NMP-based processing. The substitution of water for NMP is expected to yield significant environmental and human health benefits by mitigating the release of hazardous emissions associated with solvent recovery processes. These emissions have been found to have detrimental effects on both the environment and human well-being. The emissions were projected to be 4,400 kg for NMP-based processing, whereas only 3,400 kg were emitted during aqueous processing (Wood et al., 2017). This research examines the use of water as an alternative solvent to replace the recent toxic solvent, NMP, which is known to have significant and potentially irreversible impacts on human health and the environment. Substituting the organic system (NMP) with a water-based "aqueous system" in the cathode processing yields

advantageous outcomes. The primary objective of this study is to examine the impact of various parameters and variables related to the drying process on the energy consumption during the manufacturing of lithium-ion batteries. Additionally, the aim is to identify potential areas for optimizing energy consumption during the drying process which is represent the big portion of the energy consumption during the manufacturing process by substituting the NMP solvent with aqueous solvent (Water) without compromising battery performance at the same time it will contribute in reducing the energy consumption, CO_2 emissions and cost. The study will show the optimal values of the drying process variables which we need to achieve in order to reach the minimum energy consumption of the cathode drying process for the water based lithium ion batteries manufacturing process.

Chapter 2

LITERATURE REVIEW

2.1 Background

Replacing the conventional solvent NMP with aqueous-based technologies offers both cost savings in terms of material expenses and the potential for economically beneficial drying parameters and processes. The primary contributor of cost savings in materials is the decrease in the requirement for capital equipment and the expense of solvent recovery. Additionally, the lower price of the replacement material also contributes directly to the cost reduction. Extensive study has been conducted on the process of electrode drying, with the development of several models to assist in optimizing the removal of solvents from both anode and cathode compositions. Nevertheless, these inquiries hardly take into account the disadvantages and benefits of substituting solvents in relation to the drying of electrodes and the distribution of binders. With the increasing usage of aqueous processing for graphite anodes, numerous studies have focused on examining and improving the performance of these anodes. However, there is a lack of research on aqueous processed cathode material. There are only a few number of experiments that directly compare NMP and water, as well as determine the best drying conditions for each solvent. The optimization of drying conditions also yields tangible economic benefits. If these benefits can be achieved, the entire cell manufacturing process can be optimized, resulting in a reduction in the overall cost of the battery pack.

2.2 Cathode and Anode Drying Process

In the fabrication of electrodes, it is necessary to produce both anodes and cathodes in order to successfully finish the procedure. While the physical separation of anodes and cathodes is necessary during production, the fundamental stages of the manufacturing process remain the

same. In the production of battery pouch cells, the electrode materials, lithium manganese oxides (LMO) and graphite, are mixed with carbon black additives and binders in a solvent called N-methyl-2-pyrrolidone (NMP) at a concentration of 4% by weight. Carbon black is an additional constituent found within the electrode mixture (Yuan et al., 2017). Subsequently, the aforementioned blend is employed for the purpose of applying a layer onto a copper foil measuring 12 millimeters in thickness, intended for utilization as the graphite anode. Additionally, an alumina foil measuring 15 millimeters in thickness is coated with the same mixture, designated for application as the LMO cathode. Subsequently, the electrodes with a coating undergo a drying procedure, which is conducted at a temperature of 150 degrees Celsius for a duration of approximately ten hours (Yuan et al., 2017). Following this procedure, the subsequent stage involves the implementation of a method known as calendaring, which is employed to exert pressure on the electrodes with the aim of attaining the targeted electrode density of 10 mg/cm^2 on both the copper and alumina current collectors. During the drying stage, the solvents are extracted from the moist slurry film that has been applied to the surfaces of the current collector foils, typically copper for anodes and aluminum for cathodes. The slurry consists of the active materials that give electrochemical properties to the battery cells. The addition of the solvent in the previous step enhances the material properties both during the initial mixing stage and when the slurry is applied. Accounting for approximately 38% of the total operating costs, the drying process is identified as one of the most expensive stages in the production process. The significant energy demand covered is the main factor contributing to the high operating costs incurred. There are two distinct stages to the drying process that can be distinguished from one another. The process of solvent evaporation causes a reduction in the size of the coated layer during the first stage of the process. After that, the second phase starts when

the shrinkage stops and the solvent is evaporated through capillary transport. This marks the beginning of the second phase. The subsequent stage is primarily responsible for the movement of the binder. Because of this, it is absolutely necessary to proceed with extreme caution and take a careful approach during the drying process in order to reduce the possibility that it will cause any damage. The electrode coating is subjected to a drying process facilitated by a drying medium, typically hot dry air, which is directed over the surface of the electrode coating. The temperature of the drying medium should not exceed the saturation temperature of the solvent under atmospheric pressure (Susarla et al.). Coating shrinkage mostly happens at the beginning of the drying process, when the slurry of solid particles and solvents shrinks, making a structure with holes in it. The porous coating experiences additional shrinkage during the second stage of drying as the drying medium, in this case the ambient air, replaces the solvent in the liquid phase. In contrast to the initial phase, the subsequent drying phase exhibits a comparatively diminished reduction in coating thickness. The drying parameters show significant variation across all operations due to their dependence on factors such as the nature of the material being dried, its size and morphology, the baking process employed, the initial water content, and the permissible limits of moisture content after baking and within the cell. In general, electrodes have greater thermal stability compared to separators, enabling them to withstand elevated temperatures without experiencing detrimental effects. The temperature range in vacuum ovens, as reported, extends from 70 °C to 200 °C. The drying duration typically falls within the range of 2 to 24 hours, while the operational pressure can reach as low as 0.01 mbar (Kosfeld et al.). As the temperature increases, there is a decrease in the water content of the dried component. However, excessive drying can also have detrimental effects on the product.

2.3 Drying Parameters and variables

The complicated drying process, which is comprised of interconnected chemical and mechanical systems, requires the system to contain a large number of components and factors in order to provide an explanation that is both effective and comprehensive. This is essential in order to satisfy the requirements of this requirement. At the moment, the method that is utilized to examine the relationship between the drying parameters and the variables is the one that relies on trial and error the much more than any other way. As a consequence of this, there is an immediate need for models that can be relied upon and adapted, since this will make it easier to conduct efficient research on drying parameters and variables.

2.3.1 Drying method

Both the method and the procedure for drying have a major influence on the development of the microstructure of the electrode, as well as the cohesiveness of the film and its adherence to the current collector. Before beginning the deposition process, it is essential to make certain that the components of the electrode slurry have been properly dispersed throughout the slurry and that the active ingredients have been adequately stabilized through the use of binders and conductive additives. The utilization of a sizeable conveyor belt dryer, which is normally coupled with either an infrared heat dissipation heater or a hot air fan, is the primary method that is used in the industrial manufacture of electrodes for the purpose of drying them; this is the most common method. For the purpose of drying the pole piece in a laboratory environment, the usual procedure involves applying a slurry over the current collector. The pole piece will then dry at room temperature. When it comes to the processing of air-sensitive materials, the utilization of

inert gas flow is considered to be the most suitable method. This includes, but is not limited to, new battery materials such as high-nickel NMC and sulfide solid electrolytes with high levels of nickel. This is because inert gas flow does not react with the air in the same way that oxygen does. The presence of inert gases has the potential to speed up the drying process by making it easier for heavier gases to displace the solvents that are present in the system. The employment of spin drying has the potential to speed up the fabrication process; however, this advantage is only available for electrodes that contain particular geometries and dimensions. Spray drying is a technology that has found widespread use in a number of different commercial and industrial fields due to its capacity to achieve rapid drying rates. It is absolutely necessary to control the concentration of the water to a level that is less than 100 parts per million (ppm) (Tycorun) It is possible that the presence of water that has been left behind in the electrode can result in harmful side reactions, which will then have an effect on the overall performance of the battery. The quality and performance characteristics of battery cells are significantly influenced by the drying process of the electrodes. At present, the convection drying method is considered the most extensively employed drying technology. In addition to its significant space demands, this technology is distinguished by additional obstacles, including limited energy efficiency. Additional issues in this context encompass the presence of non-uniform heat distributions, inadequate control characteristics that include slowness and imprecision, the absence of heat alignment optimized for the materials used, a gradual increase in production rate, and the loss of heat into the surrounding workplace. Moreover, traditional drying equipment needs significant production space, adding an additional obstacle. The significant environmental impact is mostly attributed to the extensive drying sections that are necessary in conventional technologies. In order to achieve desired throughput targets, it is common practice to extend the length of dryers

to a range of 165 ft to 328 ft. (Kampker et al., 2023). To address this difficulty, a viable option involves the implementation of double-sided foil coatings combined with the utilization of long drying distances. In many cases, a multi-level dryer design or air floating units are employed to facilitate the drying process. Consequently, both options lead to a substantial increase in the complications of the equipment. The space requirements and associated expenses are frequently increased by the need for several dryer installations in order to meet specific production capabilities. Convective electrode dehumidification often employs air flotation, suction jet, or roller band dryers. Significant developments have been made in the field of laser drying technologies for electrodes, wherein the conversion of optical energy into thermal energy is achieved through the utilization of laser radiation. The utilization of photochemical and photothermal processes in this approach provides a fascinating opportunity for achieving cost reductions and enhancing the efficiency of cells (Vedder et al.). The utilization of innovative laser modules has promise for minimizing plant footprints; however, their advancement is still in the early phases of development. The wavelengths of laser beam sources show variation, covering a range from the ultraviolet to the infrared spectrum, this variability is dependent on the specific active laser medium used (Reinhart Poprawe et al.). The selection of a laser source is based on the interaction between the solvent and the substance, with the aim of achieving optimal laser radiation. The laser source, in conjunction with the beam optics, offers an extensive variety of capabilities for drying coatings. The laser source possesses a maximum output capacity exceeding 20 kilowatts per unit, enabling the application of coatings with widths that beyond existing production norms. Additionally, the laser module has the capability to cover multiple coating widths. The wavelength range covers from 790 to 1,080 nanometers (Neb et al.).

2.3.2 Drying speed

The evaporation of industrial solvents is a process that requires a substantial amount of energy, which is why it is one of the most important factors in determining the costs associated with the production of battery electrodes. It is much easier to get a well-balanced distribution of the binder material within the electrode membrane if the drying rate that is used during the fabrication procedure of the electrode is optimized to its full potential. However, a faster rate of drying may result in an uneven distribution of both liquid and dispersed binders inside the electrode. This uneven distribution could result in the accumulation of binders on the surface of the electrode, which would eventually lead to the delamination of the electrode. It is imperative to take into account both the temperature at which the drying process takes place and the thickness of the coating being applied, as these two factors have a considerable impact on the total amount of time required for the drying process. The air velocity is an essential component of the drying process, and it has a substantial impact on the total drying rate. This is due to the fact that increasing the air velocity increases the mass transfer coefficient, which in turn speeds up the drying rate. The drying rate of electrodes with an aqueous solvent (water) as opposed to NMP has a clear and significant differences due to the different between their physical and thermal properties. For example if we compare between NMP and water heat of vaporization (per mass) 513 kJ/kg and 2257 kJ/kg and the specific heat capacity 1.9 kJ/kg-K and 4.2 kJ/kg-K respectively, we will find out that water has the higher numbers. Figure (5) demonstrates a significant gap in drying rates between water and NMP, with water drying approximately 4.5 times faster than NMP (Susarla et al.). The reduced drying time leads to a lower total energy need for the operation when water is used as the solvent.

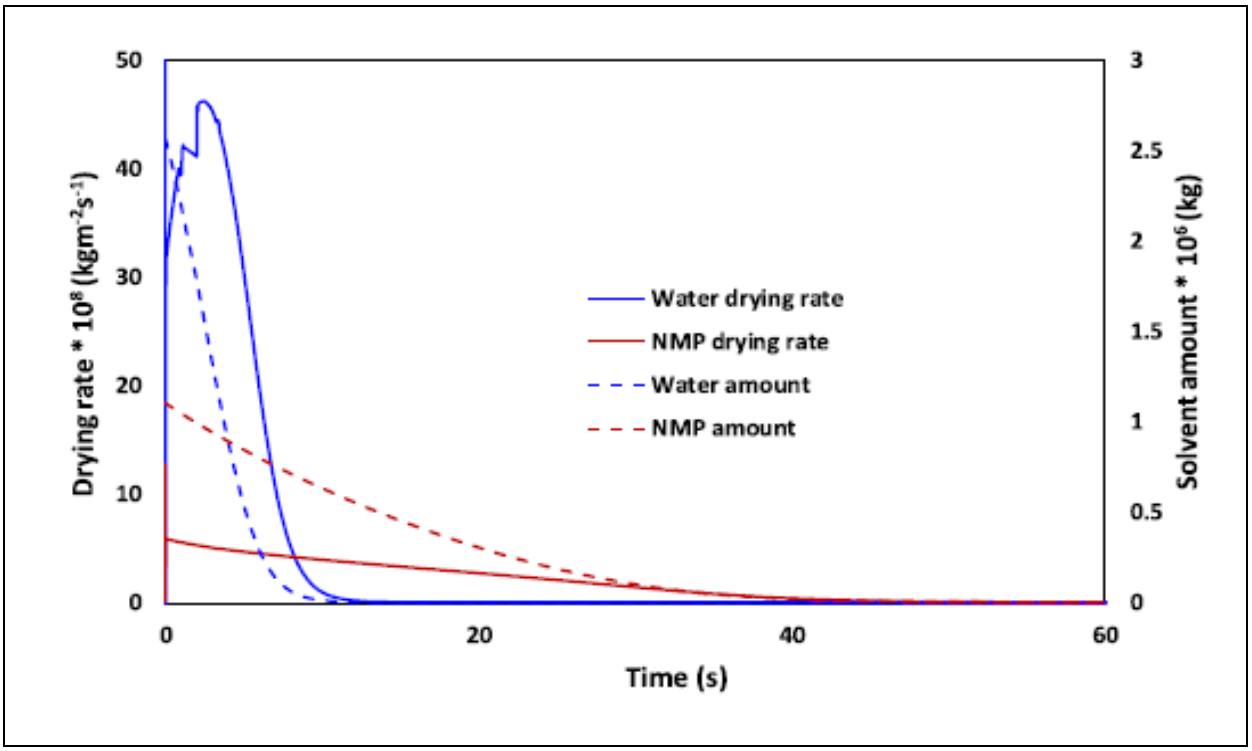

Figure 5 Drying rate profile and total solvent amount for NMP and Water (Susarla et al.).

The equilibrium vapor pressure for water is approximately 35 times higher than that of NMP, as shown in Figure (6) (Susarla et al.) it is around (93000 Pa) for water, compared to approximately (2653 Pa) for NMP. This implies that a single unit of drying air has the potential to extract 35 times more water vapor than NMP vapors, per unit volume. Due to the greater equilibrium vapor pressure, water-based electrode coatings will dry more rapidly compared to NMP-based coatings. This is because the higher vapor pressure creates a stronger driving force for water evaporation.

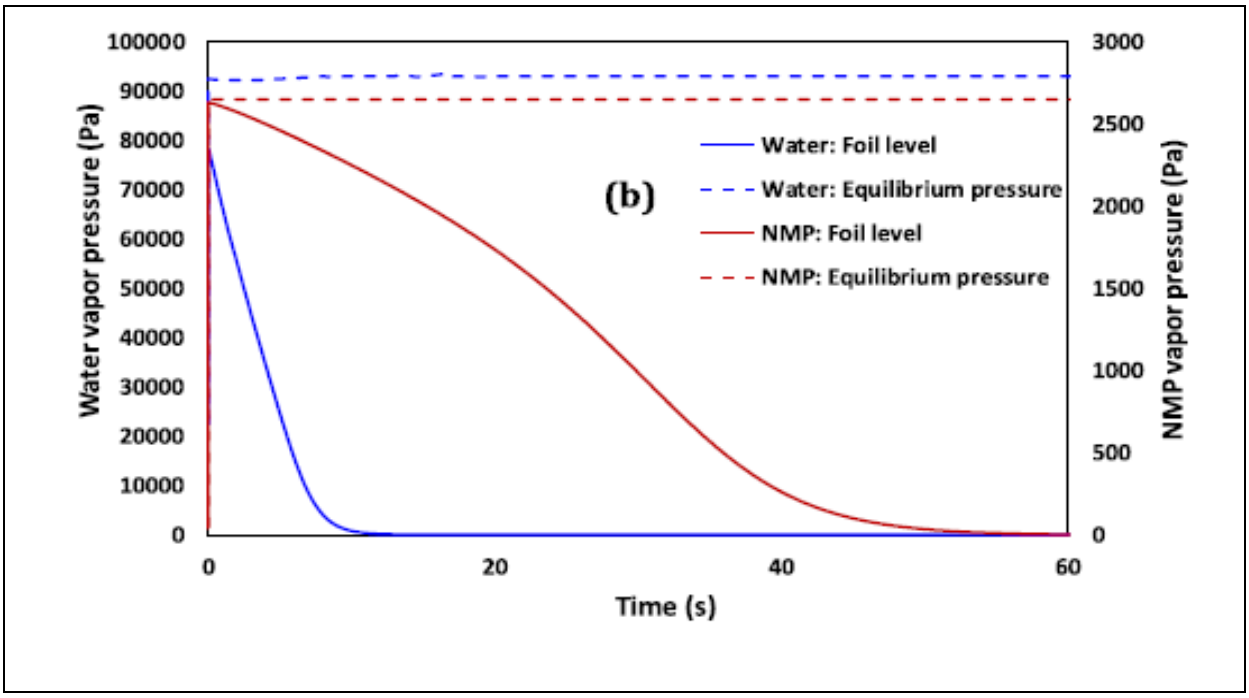

Figure 6 Vapor pressure during drying near foil level for NMP and Water (Susarla et al.).

2.3.3 Solvent type

NMP is an examples of solvent that see widespread use across a variety of industries and applications. It is anticipated that the utilization of water-based solvents will result in significant cost reductions throughout the drying and solvent recovery stages. This, in comparison to the utilization of solvents that are based on NMP, will be the case. A visible buildup of particles, an increased presence of hydroxyl groups on the surface of the coating, and a higher surface tension are some of the properties that are exhibited by the water-based slurry. In addition, it is important to note that the cathode slurry has alkaline qualities, which can cause the aluminum foil to corrode and speed up the process of metal dissolving. Both of these effects are undesirable. Efforts are underway to create water-based methods that can replace the NMP solvent in lithium ion battery production processes. Additionally, they possess the capacity to significantly decrease the drying time of the battery electrodes, thereby reducing the energy required for

manufacturing the lithium-ion battery. The Li et al. study shows that the electrochemical performance of lithium-ion battery pouch cells generated using the water-based manufacturing process is equivalent to that of lithium-ion batteries manufactured using the conventional NMP-based process (Li et al.). The Centre for Solar Energy and Hydrogen Research Baden-Württemberg (ZSW) has developed an environmentally benign and economically efficient substitute for producing cathodes on a large scale. They manufactured cathodes with a high nickel content, resulting in high specific energy and a long lifespan. This experiment was conducted on a small scale, simulating factory conditions. The electrodes obtained were then integrated into cylindrical cells of type 21700. These batteries demonstrate an exceptional ability to maintain 80 percent of their original capacity even after enduring 1,000 charge/discharge cycles, making them very appropriate for use in electric vehicles. The cells underwent 1,000 cycles of charging and discharging at a temperature of 25 degrees Celsius until their energy capacity dropped below 80 percent. Converted into driving mileage, the minimum amount covered would be 200,000 kilometers, which is the usual capacity of batteries found in modern electric automobiles ("ZSW Produces Water-Based Electrodes and Cells on a Pilot Scale"). Dr. Margret Wohlfarth-Mehrens, who is also the leader of a research group at HIU, said, "Water has long been employed as a solvent for anodes, even in large-scale industrial applications. Currently, we have achieved success in accomplishing a similar task for the cathode materials." Water not only eliminates harmful solvents but also allows for the utilization of non-fluorinated binders, hence significantly streamlining battery recycling processes. The Texas A&M Engineering Experiment Station project, which receives funding from the National Science Foundation and the U.S. Department of Energy, demonstrates that certain salt types improve the performance of the battery cathode (Luke Henkhaus 2023).

2.3.4 Thickness and Surface Load

The performance of the battery is directly influenced by the material composition of the electrode, enhancing the energy density and reducing costs can be achieved by optimizing the quantity of inactive components in a cell through the utilization of thicker electrodes. In addition, the cost can be substantially decreased through the use of aqueous electrode processing.

In order to fulfill the requirements for high energy density, lithium-ion batteries (LIBs) necessitate thick positive electrodes ranging from 100 to 200 μm. Nevertheless, it was observed that cracks extended and multiplied as the mass loading was raised. The positive electrode, which has been treated using normal aqueous solvent, has an areal loading of around 12.5 mg/cm^2 and does not contain any cracks (Rollag et al.). Cracks form when the mass loadings of the electrode exceed approximately 15 mg/cm^2. As the mass loading increased, cracks were observed expanding more extensively. When the electrode was loaded with 25 mg/cm^2, cracks showed up all the way to the aluminum foil current collector. This made it harder for the electrode to stick to the current collector and eventually came loose. The proportion of surface area covered by cracks shows a little rise for electrodes with areal mass loadings of 11 and 15 mg/cm^2. It increases from 0.00% to 0.62% and from 0.31% to 3.30%, respectively. Nevertheless, the crack intensity factor (CIF) of thick electrodes (23 mg/cm^2) exhibits a significant increase as the drying temperature rises. Specifically, it increases from 0.682% when dried at ambient temperature to 15.1% when dried at 70 °C (Rollag et al.).

Chapter 3

Model

In order to optimize and regulate the drying process, it is necessary to create a precise and succinct model. This is achieved by simplifying the problem through the use of established assumptions and simplifications. Prior to starting the drying stage, it is expected that the slurry is well blended and evenly applied onto the collectors in use. As a result, both the temperature and slurry distribution are uniform across the control volume, in both the width (x-direction) and length (y-direction) of the film. It is additionally assumed that the electrode moves consistently in the y-direction at a constant velocity. Therefore, the control volume mostly focuses on fluxes in the z-direction, specifically related to the film's height. Consequently, a one-dimensional model is obtained. The determination of the drying time for the cathode (t_{drying}) is achieved through the resolution of a dimensionless model, which is established on the basis of the subsequent set of equations, until complete evaporation of the solvent occurs. In order to get an equation for the changing thickness of the film, we utilize the principle of mass conservation on the thin film. Considering the solid densities of the components and the absence of mass transportation into the thin film, the mass balance is purely determined by the evaporation happening at the interface between the thin film and the air (Oppegård et al., 2021). The mass balance can be represented as:

$$\frac{\mathrm{d}h}{\mathrm{d}t} = -\frac{k_{\mathrm{m}} M_{\mathrm{s}}}{\rho_{\mathrm{a}} R} \cdot \left(\frac{P_{\mathrm{s}}}{T} - \frac{P_{\mathrm{a}}}{T_{\mathrm{a}}}\right) \tag{1}$$

where the variable (h) represents the thickness of the coating, (t) denotes the time, $(\mathrm{k_m})$ represents the mass transfer coefficient, $(\mathrm{M_s})$ signifies the molecular weight of the solvent, (ρ_a) Density of Air, (R) represents the ideal gas constant, (T) represents the temperature of the

coating, (T_a) represents the air temperature above the coating film, (P_a) represents the vapor pressure of the solvent in the bulk air, and (P_s) represents the equilibrium partial pressure of the solvent at the coating-air interface. (Oppegård et al., 2021).

The thin film temperature can be determined by applying the principle of energy balance to the thin film. The heat conducted away from the thin layer is equivalent to the heat required for the solvent to undergo evaporation. The heat deposited into the thin film is conveyed through either ordinary convection or radiation. In order to streamline the energy balance, we use the assumption that the film is extremely thin, resulting in rapid temperature changes within the film. As a result, we can consider the temperature to be uniform in the z-direction. In addition, the curvature of the thin film is sufficiently modest to disregard the effects of surface tension and shear stress gradients.

$$Q = -\frac{k_m M_s \lambda}{R} \cdot \left(\frac{P_s}{T} - \frac{P_a}{T_a}\right) + \dot{q}_{in} \tag{2}$$

The total energy required for the drying process is denoted by (Q). The first term in Equation (2) indicates the energy needed to remove the solvent (water) from the coating layer. Where (λ) represents the latent heat associated with the evaporation of the solvent, the second term (q_{in}) refers to the heat transferred to the coating through convection. (Oppegård et al., 2021).

3.1 Temperature

Upon examining the equation determining heat transfer via convection, it becomes evident that the initial film temperature exercises the most significant influence on energy consumption among all the parameters. The primary factor is that the energy required for the evaporation of the solvent is comparable to the energy required for heating the film. Therefore, irrespective of the quick temperature progress, the reduction in energy required for heating the film has a substantial impact on the overall energy demand. However, it is important to note that the energy saved or added during the change in initial film temperature becomes negligible when considering that this energy is either added or saved before the drying process takes place. Therefore, the initial film temperature will not affect the overall energy demand of the system, unless there are heating methods before the drying process that are more or less efficient. Moreover, the energy consumption shows a decrease when the initial temperature of the film increases. This relationship can be inferred directly from the equation, as greater temperature differences correspond to increased heat transfer. Additionally, the drying process is influenced by the air temperature in a similar manner to the initial film temperature, whereby the energy demand decreases as the air temperature increases. The previously discussed reasoning pertaining to preheating can also be applied to the ambient air temperature. The majority of studies are conducted using experimental drying temperatures within the range of 40°C (313 K) to 90°C (363 K). However, for obtaining precise findings in commercial drying, it is necessary to operate within the temperature range of 90°C (363 K) to 130°C (403 K) for water (Kukay, 2022) and from 100°C (373 K) to 180°C (453 K) in NMP case (Ahmed et al., 2016). The heat transfer resulting from convection can be mathematically represented as follows,

$$q_{in} = k_c(T_{\mathrm{a}} - T) \tag{3}$$

where (k_c) represents the heat transfer coefficient, (T) represents the temperature of the coating, (T_a) represents the air temperature above the coating film. (Oppegård et al., 2021).

The heat transfer coefficient may be determined using the provided equation (Susarla et al.). It is evident from the equation that the air velocity (V_a) significantly influences the heat transfer coefficient. Therefore, when designing the optimization model, it is extremely important to take the air velocity into consideration.

$$k_c = 0.037 V_a^{0.8} \left(\frac{\mu_a}{\rho_a}\right)^{-0.8} P_r^{1/3} L^{-0.2} \quad (4)$$

The variables in the equation are as follows:(P_r) represents the Prandtl number, (L) represents the length,(V_a) represents the air velocity, (μ_a) represents the dynamic viscosity of air, and (ρ_a) represents the air density.

3.2 Air velocity

Increasing the velocity of hot air can reduce the time required for drying by enhancing the rate of convective heat transfer. This is due to the fact that increased air velocity facilitates the more effective extraction of moisture from the material's surface, leading to accelerated evaporation. Therefore, achieving a uniform distribution of high-velocity hot air is important in order to ensure its full coverage of the entire drying material. It is important to understand that higher velocities can enhance the effectiveness of the drying process by facilitating faster moisture evaporation. Nevertheless, sustaining higher air velocities might demand a greater amount of energy input. In simple terms, higher air velocities can lead to increased operational expenses as a result of greater energy consumption. On the contrary, lower velocities may result in a longer drying period, but they need less energy. We must consider that increased air

velocities can expedite the drying process of electrode materials. Non-uniform drying or excessively quick drying can compromise the structural integrity of the cathode materials, potentially resulting in the formation of cracks.

3.3 Latent Heat

The latent heat of evaporation is the amount of energy needed to convert a liquid into vapor without any change in temperature. During the drying process of a material, such as wet items or substances with moisture, the introduction of heat triggers the evaporation process. During this phase change, the material absorbs the latent heat of evaporation, causing the liquid moisture within it to convert into vapor. Comprehending and managing this hidden heat is crucial for maximizing drying processes, since it directly impacts the energy demands and effectiveness of the entire drying operation. Maximizing the use of the heat released during evaporation is crucial for attaining ideal drying conditions, reducing energy usage, and maintaining LIB quality. Contrarily, NMP exhibits a lower heat of vaporization compared to water, with a value of (510 kJ/kg), while water has a heat of vaporization of (2260 kJ/kg). This has the potential to offer an economic benefit by providing energy input for the usage of NMP.

3.4 Thickness and Crack

The researchers support that increased drying rates and thicknesses typically result in reduced electrode uniformity and diminished final electrochemical performance. This becomes particularly evident when the temperature surpasses 350 K and the thickness rises above 150 micrometres (Bryntesen et al.).

The crack length refers to the greatest distance between the boundaries pixels of the crack. The average crack width is determined by dividing the total area of the fracture by its

length. Figure 8 (Rollag et al.) displays the average values of cracking width and length obtained from the analysis of samples subjected to specified loading mass (15 mg/cm^2) and drying temperature. The findings indicate that an elevated drying temperature results in the formation of larger and more extensive cracks. Furthermore, the range of crack lengths and widths expands as the drying temperature rises. Figure 8 displays three points indicating different probability of crack length and width values at specific temperatures (293K, 318K, and 343K) the corresponding data is presented in the table 1 below. These significant points were utilized to establish the relationship between temperature and crack dimensions. The correlation between temperature, crack width, and length is illustrated in Figure 8.

Table 1Temperature and Crack dimensions Data

Temperature (K)	Crack Length (μm)			Crack Width (μm)		
293	200	500	30	10	15	5
318	300	700	50	17	40	7
343	400	1000	70	24	60	10

The findings indicate that an elevated drying temperature results in the formation of larger and more extensive cracks. Furthermore, the range of crack lengths and widths expands as the drying temperature rises. The crack length and width are expected to increase with higher drying temperatures due to the presence of detected holes in the electrodes. No holes were present in the electrode coatings that were dried at 20 °C. As a result, the cracks were limited to a small range in terms of their length and width. It is possible that the formation of holes during the drying process at high temperatures, possibly as a result of bubbling, is what causes the increase in fracture severity as the drying temperature rises. Defects, such as holes, are recognized to facilitate the formation of cracks and act as initiation points for cracks in a thin layer.

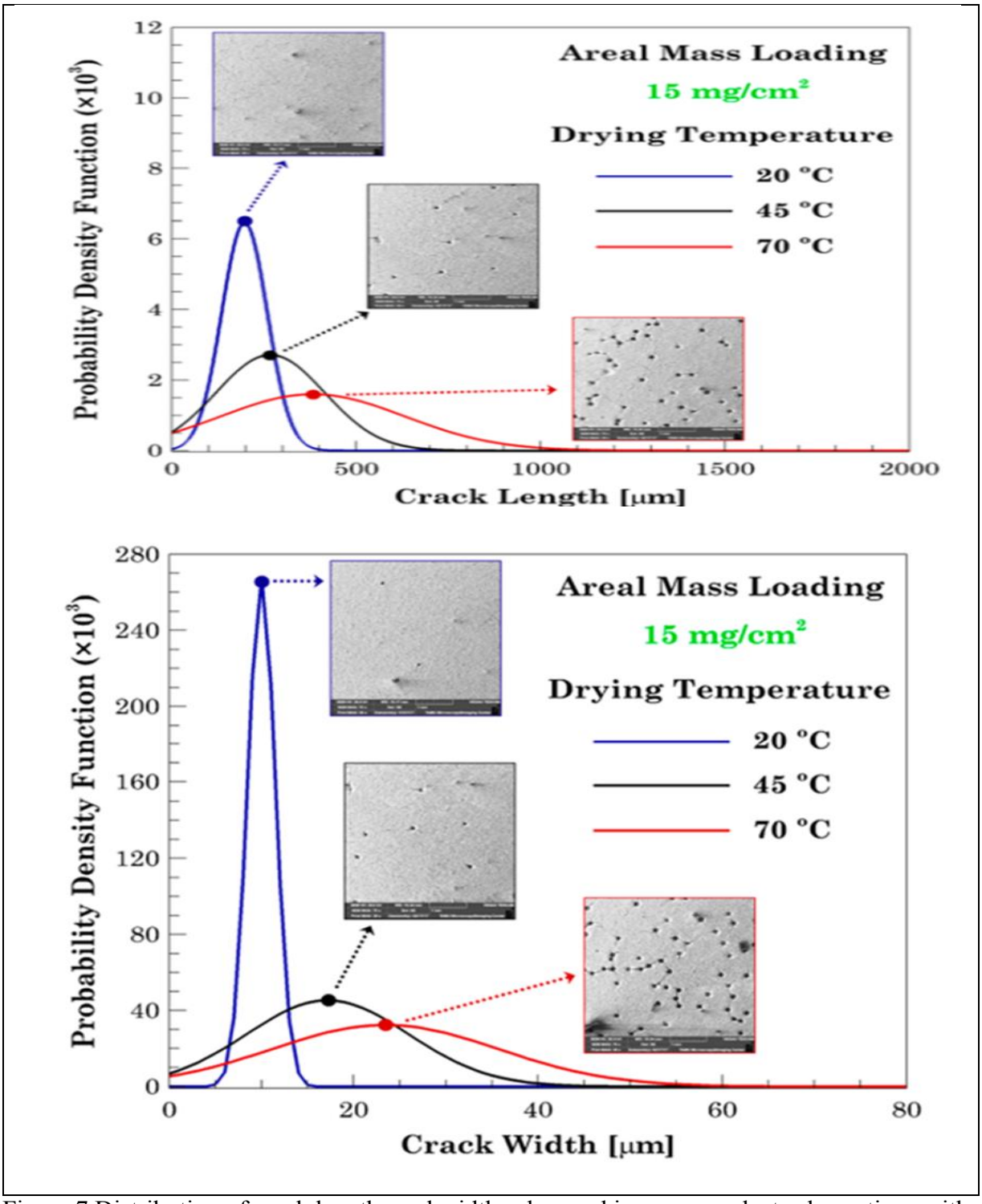

Figure 7 Distribution of crack lengths and widths observed in aqueous electrode coatings with areal mass loadings of 15 mg/cm^2

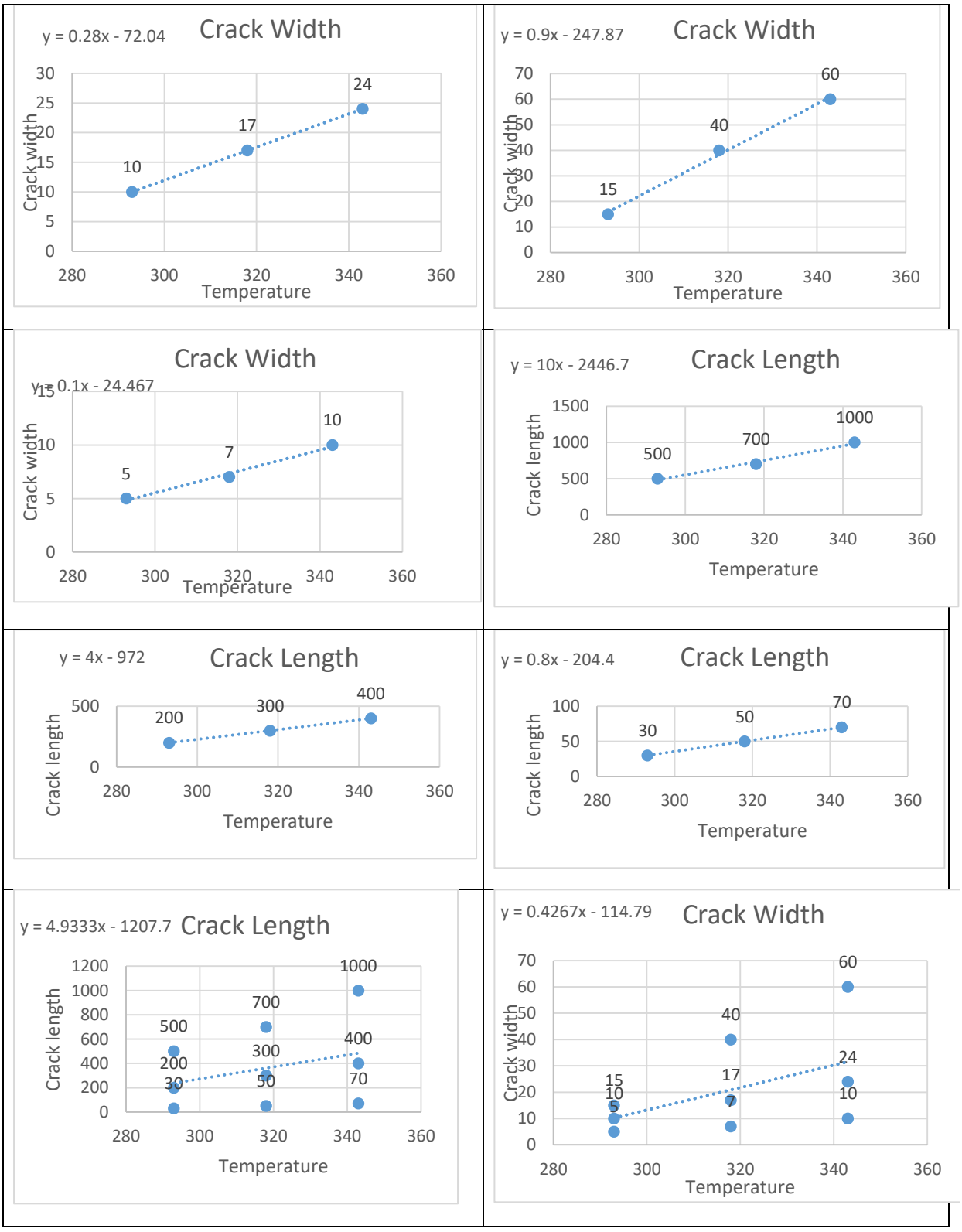

Figure 8 Correlation between temperature and crack width and length

3.5 Drying time

As that already observed Increased velocities can enhance the effectiveness of the drying process by facilitating faster moisture evaporation. Nevertheless, sustaining higher air velocities might require a greater amount of energy input. While increasing the velocity can accelerate the drying process, it may not necessarily be the most energy-efficient approach. There is a need to find a balance between the necessary duration for drying and the amount of energy consumed. Higher air velocities can lead to increased operational costs from an operating cost perspective, as they result in higher energy consumption. Conversely, reduced velocities may extend the duration of the drying process while requiring a smaller amount of energy. In order to determine the drying time required by the hot air convection dryer we will use the following equation by (EL-Mesery et al.).

$$t_{\text{drying}} = \frac{632.05 - 314.95 \ln T_a + 39.24 (\ln T_a)^2 + 0.32\, Va}{1 - 0.49 \ln T_a + 0.06 (\ln T_a)^2 + 0.002\, Va} \quad (5)$$

The equation clearly demonstrates that the air velocity (V_a) and the heated air temperature (T_a) have a substantial impact on the drying time.

3.6 Energy Consumption Model

Based upon the aforementioned equations and assumptions, it can be derived that the drying process is contingent upon two primary components: the solvent and the air. Notably, both of these factors contribute significantly to the overall energy consumption associated with this process. Firstly, the energy required to remove the solvent (water) from the coating layer. Furthermore, the energy required for heating the dry air. So we can express the energy

consumption of the drying process in terms of the solvent evaporation energy and the air heating energy (Jinasena et al., 2021).

$$E_{drying} = E_{drying(solvent)} + E_{Heating(air)} \quad (6)$$

Chapter 4

Energy Consumption Model

The drying process of electrode coatings is intrinsically intricate, as it involves the simultaneous movement of heat and mass in all three phases (solid, liquid, and gas). Transport equations that are based on the ideas of mass and energy conservation describe these transfers. To effectively model a system, it is important to comprehend the specific conditions under which the equations and assumptions used in the model hold true in a physical sense. It has to be important to clearly establish the boundaries of a mathematical model in relation to the process and physical circumstances of the system (the material being dried). Typically, the literature on drying has categorized the drying process into many sub-categories, taking into consideration elements such as the concentration of the solvent, the velocity of drying, and the amount of moisture present. The solid particles are dispersed in a solvent pool, and the process of drying primarily occurs on the surface. The rate of evaporation at the film surface, which contains the solid solvent, is the only factor in determining how quickly the solvent dries. The rate of drying in this phase, known as the constant rate period, remains constant as long as the process conditions remain unchanged.

4.1 Energy Consumption Equations

The energy consumption function that we looking for optimize it for drying lithium-ion batteries with a water-based solvent is designed and balanced to capture key energy process involved in the drying process as listed below:

1. Heat energy required to heat the battery coating that is at lower temperature than the ambient air.

2. Energy required for a phase change of the water based solvent.
3. Energy transferred to the coating through convection or radiation.

4.1.1 Energy required heating the coating

It is theorized that if the amount of energy needed for the evaporation of the solvent is similar to the amount needed for heating the film, a sudden increase in temperature would significantly decrease the energy required for film heating. Nevertheless, it is crucial to recognize that the energy change resulting from changes in the initial temperature of the film becomes insignificant when we take into account that this energy is either gained or preserved before the drying process begins. Thus, it is suggested that the starting temperature of the film has little impact on the overall energy need of the system, unless different heating methods are used prior to the drying process, which could vary in effectiveness. Therefore, the inquiry aims to clarify the relationship between the energy needed for solvent evaporation and film heating in order to optimize energy usage during the drying process. This study will not discuss the topic, but it has the potential to be a valuable subject for future debates.

4.1.2 Phase change energy

To determine the energy needed to remove the solvent (water) from the coating layer, we have to employ the following equation, which is contingent upon the mass transfer rate and latent heat of evaporation (Jinasena et al., 2021).

$$E_{drying(solvent)}=\dot{m}_{evap}\,\lambda \tag{7}$$

In this equation, ($\dot{m}_{evap}$) represents the rate when mass is lost from the thin layer as a result of evaporation, while (λ) is the latent heat of solvent evaporation.

where

$$\dot{m}_{evap} = \frac{k_m M_s}{R}\left(\frac{P_s}{T} - \frac{P_a}{T_a}\right) \quad (8)$$

$$E_{drying(solvent)=} \frac{k_m M_s}{R}\left(\frac{P_s}{T} - \frac{P_a}{T_a}\right)\lambda \quad (9)$$

4.1.3 Heat transfer energy

To calculate the energy consumed for heating the air required to complete the solvent evaporation process, we will apply the following equation (Jinasena et al., 2021).

$$E_{Heating(air)} = \ q_{in} \ = k_c(T_a - T) \quad (10)$$

Where (k_c) is the heat transfer coefficient measuring how easily heat is transferred between the coating and the surrounding air, the coefficient determines the rate of heat transfer during the drying process. On the other hand, $(T_a\text{-}T)$ is the temperature difference between heated air (T_a) and the coating film temperature (T)

By using equation (3) and equation (4), the energy need for heating air will be determine by using the following equation:

$$E_{Heating(air)} = \left(0.037 V_a^{0.8}\left(\frac{\mu_a}{\rho_a}\right)^{-0.8} P_r^{1/3} L^{-0.2}\right)(T_a - T) \quad (11)$$

The variables in the equation are as follows:(P_r) represents the Prandtl number, (L) represents the length,(V_a) represents the air velocity, (μ_a) represents the dynamic viscosity of air, and (ρ_a) represents the air density.

4.2 Optimization

The selection of optimization variables is contingent upon the aim that is to be optimized. Our objective function aims to optimize the consumption of energy. The constraints for the optimization challenge need to ensure that the technique reaches a desirable final result while also specifying upper and lower limitations on the air temperature and air velocity. This is done to prevent the outcomes from being unrealistic. One such formulation for the optimization problem concerning the amount of energy that is consumed during the drying process is as follows (Susarla et al.).:

$$E_{\text{drying}} = \frac{k_m M_s}{R}\left(\frac{P_s}{T} - \frac{P_a}{T_a}\right)\lambda + kc\,(T_a - T) \tag{12}$$

Where:

$$K_m = K_c/(\rho_{\text{a}}\ C_p)\ Le^{-\frac{2}{3}} \tag{13}$$

$$P_s = 0.6113 \exp\left(5423\left(\frac{1}{273.15} - \frac{1}{T_a}\right)\right) \tag{14}$$

$$P_a = \frac{\rho_{\text{a}}\ R\ T_{\text{a}}}{M_{\text{a}}} \tag{15}$$

The units of the parameters involved in the objective function:

(K_m) and (K_c) are dimensionless constants derived from various parameters, (Le) is Lewis number and it is dimensionless, (M_s) is the molecular weight of water (kg/kmol), (R) is the ideal gas constant (kJ/(kmol.K)), (P_s)and (P_a) are pressures (Pa), (T)and (T_a) are temperatures in Kelvin (K), (λ)is the latent heat of solvent evaporation (kJ/kg).

Objective function=$((K_m\ M_s)/\text{R})(P_s/\text{T} - P_a/T_a)\lambda + K_c(\text{T}_\text{a} - \text{T})$

Breaking it down:

(K_m) and (K_c) are dimensionless, (R*)* and (M_s) involves molecular weight and the gas constant, resulting in units of (kg/kmol) / (kJ/(kmol.K)), yielding units of K.

($P_s/T - P_a/T_a$) Yields units of (Pascal/K), (λ) is given in kJ/kg.

The resulting units of the entire objective function would be in kJ/kg, as the units of the terms involved combine to yield this unit.

Value in kWh/kg= (Objective function value in kJ/kg))(0.000277778)

4.3 Minimization problem

In order to solve the minimization problem, we want to determine the smallest amount of energy required for the drying process and identify the optimal solutions for the decision variables. Excel Solver and the parameters specified in Table 2 have been used in order to solve the objective function.

After utilizing the given equations and values to simplify the objective equation, we have derived a final formula that we will optimize, see the appendix for the derivation details.

$$\text{Minimize } E_{\text{drying}} = V_a^{0.8}\left(8.654e^{-\frac{1994.85}{T_a}} + 4.087T_a - 1197.5\right) \tag{16}$$

Subject to

$$CR_{width} = 0.28T_a - 72.04 \tag{17}$$

$$CR_{Length} = 4T_a - 972 \tag{18}$$

$$CR_{width} = 0.9T_a - 247.87 \tag{19}$$

$$CR_{Length} = 10T_a - 2446.7 \quad (20)$$

$$CR_{width} = 0.1T_a - 24.467 \quad (21)$$

$$CR_{Length} = 0.8T_a - 204.4 \quad (22)$$

$$CR_{width} = 0.4267T_a - 114.79 \quad (23)$$

$$CR_{Length} = 4T_a - 1207.7 \quad (24)$$

$$365 \leq T_a \leq 403 \quad (25)$$

$$5 \leq V_a \leq 35 \quad (26)$$

$$10 \leq CR_{width} \leq 45 \quad (27)$$

$$200 \leq CR_{Length} \leq 500 \quad (28)$$

To optimize the objective function, we need to utilize equations (17 and 18) for the first scenario, equations (19 and 20) for the second scenario, equations (21 and 22) for the third scenario, and equations (23 and 24) for the fourth scenario. For all cases, we will utilize the following equations: equation (25) from the Commercial drying range by Kukay (2022), equation (26) from the Air velocity range by Susarla et al., and equations (27 and 28) from the Crack width and length ranges by Rollag et al.

Table 2 Parameters and Decision variables

Category	Symbol	Description	Value	Unit
Decision Variables	T_a	Heated Air temperature		K
	V_a	Air velocity		m/s
Prameters				
	λ	Latent heat of solvent evaporation	2260	kJ/kg
	C_p	Heat capacity of the solvent	1900	J/KgK
	$T_{a\ min}$	Minimum temperature	365	K
	$T_{a\ max}$	Maximum temperature	403	K
	$V_{a\ min}$	Minimum air velocity	5	m/s
	$V_{a\ max}$	Maximum air velocity	35	m/s
	$t_{\text{drying-max}}$	Maximum drying time	650	s
	$t_{\text{drying-min}}$	Minimum drying time	200	s
	M_a	Molecular weights for air	28.97	Kg/Kmol
	R	Ideal gas constant	8.314	kJ /(kmol.K)
	μa	Dynamic viscosity of air	0.0000182	Pa.s
	P_r	Prandtl number	0.7	
	M_s	Molecular weights for solvent	18.015	Kg/Kmol
	ρ_a	Density of Air	1.009	Kg/m^3
	Le	Lewis number	1.19	
	L	Characteristic length	1	M
	T	Coating Film temperature	293	K
	$CR_{\text{length min}}$	Minimum Crack length	200	µm
	$CR_{\text{length max}}$	Maximum Crack length	500	µm
	$CR_{\text{width min}}$	Minimum Crack width	10	µm
	$CR_{\text{width max}}$	Maximum Crack width	45	µm

4.4 Result

The Excel Solver-based function's value of (0.580 kWh/kg and 0.718 kWh/kg) as the energy usage for drying using water as the solvent for different scenarios that we run. Given the exact conditions of a temperature (T_a) of (365 K and 380.5 K), air velocity (V_a) of (11.58 m/s and 11.85 m/s) and a drying time of (649.9 s and 650 s), this outcome demonstrates a highly effective drying process. According to the findings obtained by the Excel solver, we can conclude that the optimal scenario for minimizing energy consumption in the drying process of a water solvent is

(0.58 kWh/kg), which involves a temperature of (365 K), an air velocity of (11.58 m/s), and a drying period of (649 s). A mathematical model is developed to enhance the study of various drying techniques for electrodes, accurately determining the energy needed.

An essential aspect of comprehending the output of this model is the analysis of input uncertainties, which involves breaking them down into individual parameters. Out of these factors, the temperature of the heat source, the initial thickness, and the velocity of the air are found to be important in determining the rates of drying and the amount of energy used. Furthermore, empirical data highlights the superior energy efficiency of water as a solvent, spending significantly less energy compared to NMP, where water requires (0.58 kWh/kg), on the other hand NMP (N-Methyl-2-pyrrolidone) requires approximately (10.1 kWh/kg) for drying and solvent recovery procedures.

Table 3 Optimization Scenarios

Scenario	T_a (K)	V_a (m/s)	Energy Consumption (Kj/Kg)	Crack Width (μm)	Crack Length (μm)	drying time (s)	Energy Density (KWh/Kg)
#1	365	11.58	2088.11	30.16	488	649.99	0.58
#2	N/A	N/A	Infeasible	Infeasible	Infeasible	Infeasible	Infeasible
#3	380.5	11.85	2585.11	13.583	100	650	0.71

Chapter 5

Cost Analysis

5.1 Martials and Equipment

Within the scope of this research project, we will analyze the potential cost savings associated with switching to a water-based electrode approach from the point of view of the materials involved and the influence that this change will have on the drying process. Water has been identified as a feasible substitute for N-Methyl-2-pyrrolidone (NMP) in various applications. This is because the elimination of NMP during the drying phase of electrode coatings requires a higher level of processing energy, particularly in the form of hot air flow, compared to alternative solvents such as water and lower alcohols, these alternative solvents exhibit considerably reduced boiling temperatures and elevated vapor pressure. A significant advantage is the decreased need for drying processes as a result of the lower boiling point of water (100°C) in comparison to NMP (203°C), as well as the notably lower vapor pressure of NMP (1.0 mm Hg at 40°C) compared to water (55.3 mm Hg) (Bresser et al., 2018). Consequently, the length of the coating and drying unit can be shortened, as the evaporation rate of water is twice as high as that of NMP, this reduction in dryer length results in decreased investments in machine units. Furthermore, the recovery of NMP, a volatile organic compound (VOC), necessitates a chemical procedure such as condensation or vacuum distillation due to its poisonous, combustible, and explosive nature. This additional step significantly increases the overall expenses associated with the handling of NMP during electrode coating. The utilization of NMP in LIB electrode coating processes necessitates the implementation of measures to mitigate the risk of fire or explosion, hence leading to an augmented capital expenditure for battery plants. NMP, while classified as a combustible liquid rather than a flammable liquid, nonetheless possesses the potential to cause an explosion within a specific concentration range of

its vapor in air. The lower explosive limit (LEL) is determined to be (1.3%), whereas the maximum explosive limit is measured at (9.5%).

In the drying chamber, it is necessary to monitor the concentration of NMP to ensure that it remains equal to or below (25%) of the lower explosive limit (LEL), which is (0.325 %). In each dryer zone, it is necessary to install (LEL) monitors, which are instruments designed to measure the concentration in real time. Furthermore, the inclusion of control logic to ensure a secure operational state is also necessary. Additionally, it should be noted that the inclusion of certain units is necessary for N-Methyl-2-pyrrolidone (NMP) processing, but they are not required for water treatment. These units include: a condenser; a zeolite wheel; a scrubber; NMP storage tanks; and chillers and heaters to facilitate NMP recovery. The examination of the NMP recovery process has been initiated through the establishment of a process model. Figure 10 (Wood et al., 2017) illustrates a process flow diagram demonstrating the sequential recovery of the evaporated solvent from the dryer. Initially, the solvent is condensed in a condenser, followed by its subsequent capture on a zeolite wheel. Finally, the solvent is effectively removed from the exhaust by a scrubbing process. In the context of a high-volume production scenario, the elimination of solvent recovery and missions equipment yields substantial cost reductions in capital expenditure for manufacturing facilities, ranging from $3 to $6 million (Wood et al., 2017), to provide greater precision or specificity the annual expenditure for the NMP recovery process totals $4.6 million, equivalent to ($45.8 per pack) or ($1.12 per kilogram of NMP) (Ahmed et al., 2016). Table 4 below has been created in accordance with the 2017 study by Wood et al. This table displays the projected capital cost for the NMP recovery process. However, if we use water as a solvent instead of NMP, we will avoid this expense and save $5.09 million.

Table 4 Estimated NMP Recovery Equipment Costs

Equipment	Estimated Industrial cost
NMP storage tank	$560,000
Main blower	$190,000
Make-up air blower	$36,500
Distillation column	$1,000,000
Air-to-air heat exchanger	$460,000
Zeolite wheel	$425,000
Filter	$14,000
Scrubber	$25,000
Air heater	$20,000
Condenser	$1,380,000
Chiller	$950,000
Chilled water pump	$25,000
Total Cost	$5,085,500

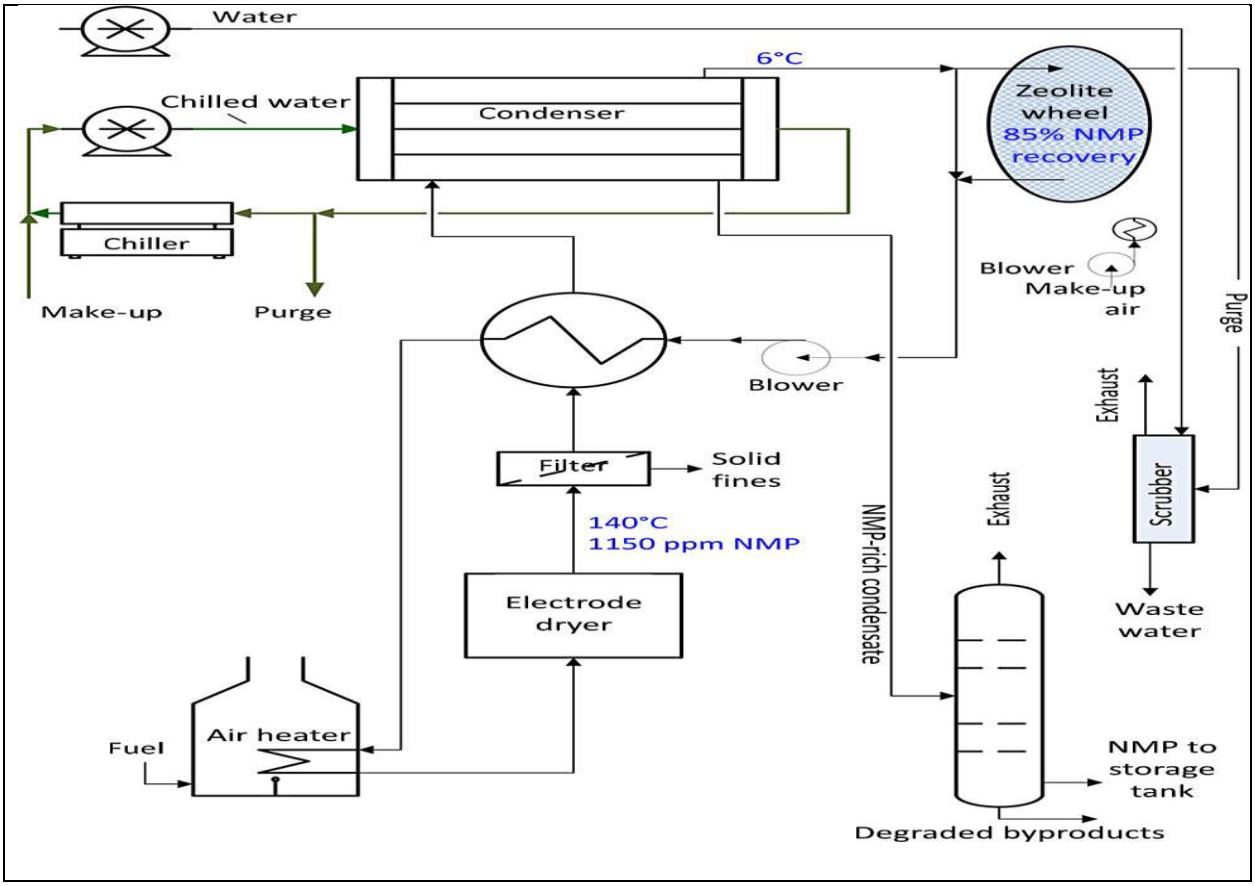

Figure 9 Schematic of a typical process for the drying and recovery of NMP (Wood et al., 2017).

5.2 Energy Consumption Saving

As previously stated, the elimination of the solvent recovery process and its associated equipment would result in cost savings in terms of capital investment. Additionally, there would be a reduction in energy usage, as this process is known to be energy-intensive. The concentration of NMP vapor in the gas phase must be kept much below the lower flammability limit, which is approximately (1.1%) at a temperature of 140°C (Ahmed et al., 2016). The previously mentioned limitation necessitates the utilization of a substantial quantity of hot air in order to facilitate the drying procedure. Significant energy consumption arises due to the substantial volume of air that needs heating and cooling. The necessity for a significant volume of air flow arises from the requirement to maintain the concentration of NMP (1,150 ppmv) in the dryer at a significantly lower level than the flammability limit. Water has a greater heat of vaporization (per unit mass) and specific heat capacity compared to N-Methyl-2-pyrrolidone (NMP); yet, water has the ability to undergo drying processes approximately 4.5 times more rapidly than NMP. Water exhibits a drying rate that is 4.5 times more rapid than NMP (Susarla et al., 2018b), while possessing a greater heat of vaporization (per unit mass) and specific heat capacity. The utilization of water as a solvent in the process requires a greater quantity of energy for vaporization. However, due to the reduced duration of the drying process, the overall energy consumption is lower compared to alternative methods. Based on the previous section's findings, which indicate that the total energy required for the drying process is 0.58 kWh/kg, we can conclude that by using water as a solvent instead of NMP solvent (which requires 10.2 kWh/kg), We can achieve a reduction in energy usage of over 10 times during the drying process, as confirmed by (Susarla et al) in his experimental study, Table 5 shows the cost analysis for 57 kWh battery pack by using NMP and water-based solvents (Yuan et al., 2017).

Table 5 Cost factors of the NMP& Water drying

Solvent	Energy Density(KWh/Kg)	Quantity (Kg)/Pack	Energy For drying (KWh)	Natural Gas Cost/KWh	Natural Gas Cost/Pack	Material Cost/Kg	Total material cost/pack
Water	0.58	120	69.6	$0.02	$1.392	$0.2	$24
NMP	10.2	35	357	$0.02	$7.14	$2.5	$87.5

Table 6 Solvents Properties Comparison

	Water	NMP
Material Cost	$0.2/L	$2.5/L
Solvent Recovery System	N/A	$5,085,500
Boling Point	100 C	204 C
Vapor Pressure	Higher	Lower
Drying Rate	Higher	Lower
Drying Time	Lower (4.5 faster)	Higher
Energy consumption for drying	0.58 KWh/Kg	10.2 KWh/Kg
Toxic	Nontoxic	Toxic
CO2 Emissions	Lower	Higher
Flammability	Non-Flammable	Flammable
Capacity retention	83.7% after 668 cycles.	79.5 after 886 cycles

Chapter 6

Conclusion

A mathematical model is being developed to simplify the analysis of different drying methods for electrodes and to accurately estimate the amount of energy needed. In order to determine the parameters that have the largest impact on the created model output, it is essential to analyze the input uncertainty by breaking it down into its many parameters. The temperature of the heat source, and the air velocity are the most critical elements affecting both the drying rate and energy consumption. Furthermore, it has been proven that using water as a solvent consumes less energy compared to using NMP as a solvent, Table 6 bellow shows the major differences between the two solvents. The energy consumption of water is 0.58 kilowatt hours per kilogram, on the other hand, (Ahmed et al., 2016) developed a spreadsheet model is utilized to analyze the energy requirements for drying the coated cathode layer and recovering the solvent (NMP). The base case scenario reveals that the drying and recovery process necessitates approximately 10 kWh of energy per kilogram of solvent (NMP). The potential of this model include the optimization of energy usage, minimizing costs, and developing controls that manage drying activities. With the increasing interest in manufacturing LIB electrodes, particularly cathodes, using water-based slurries, one of the main issues related to its implementation, namely slurry wetting and agglomeration, have been resolved by ORNL. However, battery makers and automotive OEMs still have one concern: does aqueous processing contribute significantly to the moisture that is chemisorbed and physisorbed prior to the secondary drying step, leading to higher capacity fade during long-term cycling, the matter has recently been tackled at Oak Ridge National Laboratory (ORNL). Additional improvements utilizing life cycle assessment models could provide a more precise and thorough knowledge. This comprehensive investigation may

involve several drying methodologies and categories of lithium-ion batteries, elucidating knowledge about energy usage, emissions of greenhouse gases, and economic considerations. This research offers detailed information on the drying processes of different technologies and LIB kinds, enabling educated decision-making in line with sustainable practices. The comprehensive perspective obtained by analyzing energy usage, emissions, and cost establishes the foundation for ethical and efficient drying methods in the field of lithium-ion batteries (LIBs). The expansion of this research to encompass comprehensive life cycle assessment models has the potential to significantly impact the sustainable development of lithium-ion batteries (LIBs). This extensive investigation has the potential to uncover valuable and essential insights that go beyond the immediate focus by exploring different drying processes and various types of LIBs.

APPENDIX

Abbreviations Table

Abbreviation	Definition
EV	Electronic Vehicles
NMP	N-Methyl-2-pyrrolidone
LIB	lithium-ion battery
LiCoO2	lithium cobalt oxide
SEI	Solid Electrolyte Interface
GWP	Global Warning Potential
kWh (el)	Kilo watt per hour of electric
kWh (c)	Kilo watt per hour of cell
VOC	volatile organic compound
BatPaC	battery pack cost estimated
LEL	lower explosive limit
KWH	Kilo watt per hour
KWh/Kg	Kilo watt per hour per Kg
T_a	Heated Air temperature
V_a	Air velocity
P_s	Equilibrium vapor pressure of the solvent
P_a	Partial pressure of Air
$t_{drying\text{-}max}$	Maximum drying time
$t_{drying\text{-}min}$	Minimum drying time
λ	Latent heat of solvent evaporation
Cp	Heat capacity of the solvent
R	Ideal gas constant
μa	Dynamic viscosity of air
Pr	Prandtl number
M_s	Molecular weights for solvent
ρ_a	Density of Air
Le	Lewis number
L	Characteristic length
T	Coating Film temperature
$CR_{length\ min}$	Minimum Crack length
$CR_{length\ max}$	Maximum Crack length
$CR_{width\ min}$	Minimum Crack width
$CR_{width\ max}$	Maximum Crack width

Equations Derivation

$$P_a = \frac{\rho_{\mathrm{a}}\ R\ T_{\mathrm{a}}}{M_{\mathrm{a}}}$$

Substitute the given values for(R), (ρ_{a}) and (M_{a}):

$$P_a = (1.009)\ (8.314)T_{\mathrm{a}}/28.97$$

$$P_a = (28.97)(1.009)/8.314T_{\mathrm{a}}$$

Simplify the expression:

$$P_a = (8.284126)T_{\mathrm{a}}/28.97$$

Now, you have a simplified expression for P_a:

P_a =0.286 T_{a}

Also,

$$P_s = 0.6113 \exp\left(5423\left(\frac{1}{273.15} - \frac{1}{T_a}\right)\right)$$

Start with the given expression:

$$P_s = 0.6113e^{5423\left(\frac{1}{273.15} - \frac{1}{T_a}\right)}$$

Combine the fractions in the exponent:

$$P_s = 0.6113e^{5423\frac{T_a - 273.15}{273.15T_a}}$$

Expand the exponent using the property $a^{b/c} = (a^b)^{1/c}$:

$$P_s = 0.6113e^{\frac{5423(T_a - 273.15)}{273.15T_a}}$$

Split the exponent into two terms:

$$P_s = 0.6113e^{\frac{5423T_a}{273.15T_a} - \frac{(523)(273.15)}{273.15T_a}}$$

Simplify each term separately:

$P_s = 0.6113e^{19.85-\frac{5423\times273.15}{273.15T_a}}$

$P_s = 0.6113e^{19.85-\frac{5423\times273.15}{27.3.15T_a}}$

Combine the constants in the exponent:

$P_s = 0.6113e^{19.85-1994.85/T_a}$

Now, you can further simplify the expression by moving the constant term outside the exponential:

$P_s = 0.6113e^{19.85}(e^{-\frac{1994.85}{T_a}})$

Combine the constants:

$P_s = 1.077e^{-1994.85/T_a}$

So, the further simplified expression for P_s is:

$P_s = 1.077e^{-1994.85/T_a}$

Now, we have

$K_c = 0.037{V_a}^{0.8}\left(\frac{\mu_u}{\rho_a}\right)^{-0.8}\mathrm{Pr}^{1/3}L^{-0.2}$

Substitute the given values for μ_a, P_r, ρ_a, and L :

$K_c = 0.037{V_a}^{0.8}\left(\frac{0.0000182}{1.009}\right)^{-0.8}(0.7^{1/3})(1^{-0.2})$

Now, simplify the expression:

$K_c = 0.037{V_a}^{0.8}((0.00001801)^{-0.8})(0.866)$

Further simplify:

$K_c = (0.037)({V_a}^{0.8})(110.491)$

$K_c = 4.087{V_a}^{0.8}$

Finally, To solve for K_m in the equation $K_m = \frac{K_c}{\rho_a C_p}Le^{-\frac{2}{3}}$, where $\rho_a = 1.009, C_p = 1900$, and $Le = 1.19$, you can follow these steps:

Start with the given equation:

$$K_m = \frac{K_c}{\rho_a C_p} Le^{-\frac{2}{3}}$$

Substitute the given values for ρ_a, C_p, and Le :

$$K_m = \frac{K_c}{(1.009)(1900)} 1.19^{-\frac{2}{3}}$$

Simplify the expression:

$$K_m = \frac{K_c}{1918.1} 0.833$$

$$K_m = \frac{K_c(0.833)}{1918.1}$$

So, the expression for K_m after substitute K_c is:

$$K_m = \frac{(4.087)({V_a}^{0.8})(0.833)}{1918.1}$$

$$K_m = \frac{3.406{V_a}^{0.8}}{1918.1}$$

$$K_m = 0.00177{V_a}^{0.8}$$

simplify the expression $\frac{K_m M_s}{R}$ using the given values $R = 8.314$ and $M_s = 18.015$, and the previously derived expression for K_m :

$$K_m = \frac{{V_a}^{0.8}}{563.52}$$

Now, substitute these values into the expression:

$$\frac{K_m M_s}{R} = \frac{\frac{{V_a}^{0.8}}{563.52} 18.015}{8.314}$$

Simplify the expression:

$$\frac{K_m M_s}{R} = \frac{0.032{V_a}^{0.8}}{8.314}$$

Now, we have the simplified expression for $\frac{K_m M_s}{R}$:

$\frac{K_m M_s}{R} = \frac{0.032 \cdot {V_a}^{0.8}}{8.314} = (0.0038 {V_a}^{0.8})$

Now, for the main objective function we will substitute P_a and P_s into the main expression:

$= (0.0038 {V_a}^{0.8}) \left(\frac{1.077 \times e^{-1994.85/T_a}}{293} - \frac{0.286\ T_a}{T_a}\right) 2260 + 4.087\ {V_a}^{0.8} (T_a - 293)$

$= (0.0038. {V_a}^{0.8}) \left(\frac{1.077 \times e^{-1994.85/T_a}}{293} - \frac{0.286\ T_a}{T_a}\right). 2260 + 4.087\ {V_a}^{0.8} (T_a - 293)$

combine terms involving $V_a^{0.8}$ in the expression:

$= 0.0038 V_a^{0.8} \left(\frac{1.077 e^{\frac{1904.85}{T_a}}}{293} - 0.286\right) 2260 + 4.087 V_a^{0.8} (T_a - 293)$

Combining terms involving $V_a^{0.8}$:

$= V_a^{0.8} \left(0.0038 \left(\frac{1.077 e^{\frac{184.s}{T_a}}}{293} - 0.286\right) 2260 + 4.087 (T_a - 293)\right)$

combine terms involving T_a in the expression:

$= V_a^{0.8} \left(0.0038 \left(\frac{1.077 \cdot e^{-1994 \frac{184}{T_a}}}{293} - 0.286\right) 2260 + 4.087 (T_a - 293)\right)$

Combining terms involving T_a :

$= V_a^{0.8} \left(0.0038 \frac{1.077 e^{-\frac{1904.85}{T_a}}}{293} * 2260 + 4.087 T_a - (4.087)(293)\right)$

$= V_a^{0.8} \left(0.0038 \frac{1.077 \cdot e^{-1994.85/T_a}}{293} \cdot 2260 + 4.087 T_a - (4.087)(293)\right)$

Combine constants:

$= V_a^{0.8} \left(8.654 e^{-\frac{1994.85}{T_a}} + 4.087 T_a - 1197.5\right)$

References

McManus, M. C. (2012, January 13). *Environmental consequences of the use of batteries in low carbon systems: The impact of battery production*. Applied Energy. https://www.sciencedirect.com/science/article/abs/pii/S0306261911008580?via%3Dihub

The United States Government. (2021, November 8). *Fact sheet: The bipartisan infrastructure deal boosts clean energy jobs, strengthens resilience, and advances environmental justice*. The White House. https://www.whitehouse.gov/briefing-room/statements-releases/2021/11/08/fact-sheet-the-bipartisan-infrastructure-deal-boosts-clean-energy-jobs-strengthens-resilience-and-advances-environmental-justice/

Henze, V. (2022, December 6). *Lithium-ion battery pack prices rise for first time to an average of $151/kwh*. BloombergNEF. https://about.bnef.com/blog/lithium-ion-battery-pack-prices-rise-for-first-time-to-an-average-of-151-kwh/

Duffner, F., Mauler, L., Wentker, M., Leker, J., & Winter, M. (2021). Large-scale automotive battery cell manufacturing: Analyzing strategic and operational effects on manufacturing costs. *International Journal of Production Economics*, *232*, 107982. https://doi.org/10.1016/j.ijpe.2020.107982

Kukay, A. (2022). Optimizing Aqueous Processing of Nickel-Rich Cathode Material in Ultra-Thick Lithium-IonBatteries.*DoctoralDissertations*.https://trace.tennessee.edu/utk_graddiss/7132/

Tesla. Energy.gov. (n.d.). https://www.energy.gov/lpo/tesla#:~:text=In%20January%202010%2C%20the%20Department,for%20powering%20specially%20designed%20all%2D

Conlon, D. (2022, February 10). *Electric-car battery manufacturing plants and recyclers: What's in store for the U.S.* ALL4. https://www.all4inc.com/4-the-record-articles/electric-car-battery-manufacturing-plants-and-recyclers-whats-in-store-for-the-u-s/

Gupta, N. (2021, June 11). *Li-ion cell manufacturing: A look at processes and equipment*. Emerging Technology News. https://etn.news/energy-storage/li-ion-cell-manufacturing#:~:text=The%20production%20of%20the%20lithium,and%20testing%20the%20battery%20cells.

Thomitzek, M., Cerdas, F., Thiede, S., & Herrmann, C. (2019). Cradle-to-gate analysis of the embodied energy in lithium ion batteries. *Procedia CIRP*, *80*, 304–309. https://doi.org/10.1016/j.procir.2019.01.099

Guo, Y. (2009). Safety | thermal runaway. *Encyclopedia of Electrochemical Power Sources*, 241–253. https://doi.org/10.1016/b978-044452745-5.00394-4

Jinasena, A., Burheim, O. S., & Strømman, A. H. (2021). A flexible model for benchmarking the energy usage of automotive lithium-ion battery cell manufacturing. *Batteries*, *7*(1), 14. https://doi.org/10.3390/batteries7010014

Nigel. (2022, October 11). Energy used to Manufacture a Cell. Battery Design. https://www.batterydesign.net/energy-used-to-manufacture-a-cell/

Makrides, G., Zinsser, B., Norton, M., Georghiou, G. E., Schubert, M., & Werner, J. H. (2010). Potential of photovoltaic systems in countries with high solar irradiation. *Renewable and Sustainable Energy Reviews*, *14*(2), 754–762. https://doi.org/10.1016/j.rser.2009.07.021

Yuan, C., Deng, Y., Li, T., & Yang, F. (2017). Manufacturing energy analysis of lithium ion battery pack for electric vehicles. *CIRP Annals*, *66*(1), 53–56. https://doi.org/10.1016/j.cirp.2017.04.109

Li, Jianlin, et al. "Water-Based Electrode Manufacturing and Direct Recycling of Lithium-Ion Battery Electrodes—a Green and Sustainable Manufacturing System." *IScience*, vol. 23, no. 5,May 2020, p. 101081, https://doi.org/10.1016/j.isci.2020.101081

Susarla, Naresh, et al. "Modeling and Analysis of Solvent Removal during Li-Ion Battery Electrode Drying." *Journal of Power Sources*, vol. 378, Feb. 2018, pp. 660–670, https://doi.org/10.1016/j.jpowsour.

Son, Hye Bin, et al. "A Dry Room-Free High-Energy Density Lithium-Ion Batteries Enabled by Impurity Scavenging Separator Membrane." *Energy Storage Materials*, vol. 36, 1 Apr. 2021, pp. 355–364, www.sciencedirect.com/science/article/abs/pii/S2405829721000192?fr=RR-1&ref=cra_js_challenge, https://doi.org/10.1016/j.ensm.2021.01.018.

"Battery - Munters." *Www.munters.com*, www.munters.com/en-us/industries/battery/.

Kosfeld, Malte, et al. "Moisture Behavior of Lithium-Ion Battery Components along the Production Process." *Journal of Energy Storage*, vol. 57, Jan. 2023, p. 106174, https://doi.org/10.1016/j.est.2022.106174.

SMITH, JR., ROBERT. "Advanced Dry Room Concept." *Www.harrisenv.com*, www.harrisenv.com/korea_paper.htm.

Tycorun. "Drying Process Mechanism and Test Method of Battery Pole Piece." *Tycorun Batteries*, 30 Jan. 2023, www.tycorun.com/blogs/news/drying-process-mechanism-of-battery-pole-piece.

Bresser, D., Buchholz, D., Moretti, A., Varzi, A., & Passerini, S. (2018). Alternative binders for sustainable electrochemical energy storage – the transition to aqueous electrode processing and bio-derived polymers. *Energy & Environmental Science*, *11*(11), 3096–3127. https://doi.org/10.1039/c8ee00640g

Duffner, F. (2021). Large-scale automotive battery cell manufacturing: Analyzing strategic and operational effects on manufacturing costs. *International Journal of Production Economics*, *232*, 107982. https://doi.org/10.1016/j.ijpe.2020.107982

Wood, D. L., Quass, J. D., Li, J., Ahmed, S., Ventola, D., & Daniel, C. (2017). Technical and economic analysis of solvent-based lithium-ion electrode drying with water and NMP. *Drying Technology*, *36*(2), 234–244. https://doi.org/10.1080/07373937.2017.1319855

Ahmed, S., Nelson, P. A., Gallagher, K. G., & Dees, D. W. (2016). Energy impact of cathode drying and solvent recovery during lithium-ion battery manufacturing. Journal of Power Sources, 322, 169–178. https://doi.org/10.1016/j.jpowsour.2016.04.102

Kampker, A., Heimes, H., Dorn, B., & Hendel, R. (2023, May 22). Diode Laser Drying of ElectrodesforLithiumIonBatteries.ResearchGate.https://www.researchgate.net/publication /370953875_Diode_Laser_Drying_of_Electrodes_for_Lithium-Ion_Batteries

Neb, Daniel, et al. "Current Advances on Laser Drying of Electrodes for Lithium-Ion Battery Cells." *Procedia CIRP*, vol. 107, 1 Jan. 2022, pp. 1577–1587, www.sciencedirect.com/science/article/pii/S2212827122004784, https://doi.org/10.1016/j.procir.2022.05.194. 2

Vedder, Christian, et al. *Laser-Based Drying of Battery Electrode Layers*. 1 Jan. 2016, https://doi.org/10.2351/1.5118636.

Reinhart Poprawe, et al. *Tailored Light 1*. Springer, 5 Apr. 2018.

Wolf, Sebastian, et al. "Process and Material Analysis of Laser- and Convection-Dried Silicon–Graphite Anodes for Lithium-Ion Batteries." *World Electric Vehicle Journal*, vol. 14, no. 4, 1 Apr. 2023, p. 87, www.mdpi.com/2032-6653/14/4/87, https://doi.org/10.3390/wevj14040087.

Oppegård, Emil, et al. "Study of an Industrial Electrode Dryer of a Lithium-Ion Battery Manufacturing Plant: Dynamic Modelling." *Easychair.org*, 2 Oct. 2020, easychair.org/publications/preprint/Dp1S.

Oppegård, Emil. "Optimization and Control of Battery Electrode Drying Process." *Ntnuopen.ntnu.no*, 2021, ntnuopen.ntnu.no/ntnu-xmlui/handle/11250/2781024.

Mesbah, Ali, et al. "Nonlinear Model-Based Control of Thin-Film Drying for Continuous Pharmaceutical Manufacturing." *Industrial & Engineering Chemistry Research*, vol. 53, no. 18, 31 Dec. 2013, pp. 7447–7460, https://doi.org/10.1021/ie402837c.

EL-Mesery, Hany S., et al. "Evaluation of Infrared Radiation Combined with Hot Air Convection for Energy-Efficient Drying of Biomass." Energies, vol. 12, no. 14, 1 Jan. 2019, p. 2818, www.mdpi.com/1996-1073/12/14/2818, https://doi.org/10.3390/en12142818.

Rollag, Kelsey, et al. “Drying Temperature and Capillarity-Driven Crack Formation in Aqueous Processing of Li-Ion Battery Electrodes.” *ACS Applied Energy Materials*, vol. 2, no. 6, 3 June 2019, pp. 4464–4476, https://doi.org/10.1021/acsaem.9b00704.

Bryntesen, Silje Nornes, et al. “Opportunities for the State-of-The-Art Production of LIB Electrodes—a Review.” Energies, vol. 14, no. 5, 4 Mar. 2021, p. 1406, https://doi.org/10.3390/en14051406

“ZSW Produces Water-Based Electrodes and Cells on a Pilot Scale.” *Helmholtz-Institut Ulm*, hiu- batteries.de/en/news_and_events/zsw-produces-water-based-electrodes-and-cells-on-a-pilot-scale/.

luke.henkhaus. (2023, April 5). Texas A&M Researchers Find Major Storage Capacity In Water-Based Batteries. Texas A&M Today. https://today.tamu.edu/2023/04/05/texas-am-researchers-find-major-storage-capacity-in-water-based-batteries/

Jinasena, A., Burheim, O. S., & Strømman, A. H. (2021). A Flexible Model for Benchmarking the Energy Usage of Automotive Lithium-Ion Battery Cell Manufacturing. Batteries, 7(1), 14. https://doi.org/10.3390/batteries7010014